# QUALITY INFORMATION DOCUMENT

# for the Black Sea Waves Reanalysis Product BLKSEA_REANALYSIS_WAV_007_006

**Issue:** 0

**Contributors:** Arno Behrens, Oliver Krueger, Joanna Staneva, Elisaveta Peneva

**CMEMS version scope :** Version 1.0

**Approval date by the CMEMS product quality coordination team: dd/mm/yyyy**

# CHANGE RECORD

When the quality of the products changes, the QuID is updated and a row is added to this table. The third column specifies which sections or sub-sections have been updated. The fourth column should mention the version of the product to which the change applies.

| Issue | Date | § | Description of Change | Author | Validated By |
|---|---|---|---|---|---|
| 1.0 | 02/02/2018 | All | First version of document of CMEMS V4 | A. Behrens, O. Krueger, J. Staneva | E. Peneva |
| | | | | | |
| | | | | | |

# TABLE OF CONTENTS


*I Executive summary* ..... *7*

I.1 Products covered by this document ..... 7

I.2 Summary of the results ..... 7

I.3 Estimated Accuracy Numbers ..... 8

*II Production system description* ..... *9*

II.1 Production centre details ..... 9

II.2 System Description ..... 10

*III Validation framework* ..... *14*

III.1 Quality control of the satellite data ..... 14

III.2 Statistical analysis ..... 14

III.3 Time series analysis ..... 15

III.4 Spatial statistics ..... 16

*IV Validation results* ..... *17*

IV.1 Statistical analysis ..... 17

IV.2 Comparison with Pasha Dere ..... 19

IV.3 Time series analysis ..... 21

IV.4 Spatial statistics ..... 23

*V Examples* ..... *34*

*VI System's Noticeable events, outages or changes* ..... *41*

*VII Quality changes since previous version* ..... *42*

*VIII References* ..... *43*

# LIST OF FIGURES


FIGURE 1: BLACK SEA WAVE MODEL WAM DEPTH DISTRIBUTION ..... 10

FIGURE 2: SCATTER PLOTS SHOWING SATELLITE MEASUREMENTS VERSUS MODELLED SIGNIFICANT WAVE HEIGHTS FOR THE PERIODS 15.01.2002-20.06.2013 (JASON-1), 04.07.2008-15.07.2017 (JASON-2), 13.02.2016-02.11.2017 (JASON-3), AND 15.01.2002-02.11.2017 (ALL SATELLITES MERGED). ALSO SHOWN ARE THE ESTIMATED BIVARIATE PROBABILITY DENSITY, THE LINEAR SLOPE-FIT REGRESSION OF MODELLED AND OBSERVED WAVE HEIGHTS, AND SPECIFIC QUANTILES TAKEN FROM THE EMPIRICAL CUMULATIVE DENSITY FUNCTION. FURTHERMORE, SUMMARY STATISTICS AND SKILL SCORES ARE INCLUDED. ..... 17

FIGURE 3: SIGNIFICANT WAVE HEIGHT AND PEAK PERIOD FROM WAM AND FROM THE ADCP STATION PASHA DERE IN THE PERIOD 04-15 FEBRUARY 2012. ..... 19

FIGURE 4: TIME SERIES OF ANNUAL MINIMUM, MEAN, AND MAXIMUM SIGNIFICANT WAVE HEIGHTS, AS WELL AS TIME SERIES OF SPECIFIC ANNUAL QUANTILES OF SIGNIFICANT WAVE HEIGHTS DERIVED FROM JASON SATELLITE MEASUREMENTS AND FROM WAM. ..... 21

FIGURE 5: UPPER ANNUAL QUANTILES OF SIGNIFICANT WAVE HEIGHTS DERIVED FROM SATELLITE MEASUREMENTS AND WAM. ..... 23

FIGURE 6: NUMBER OF VALID COMBINED SATELLITE OBSERVATIONS FROM JASON-1, JASON-2, AND JASON-3 PER GRID CELL WITHIN THE PERIOD 15.01.2002-02.11.2017. ..... 24

FIGURE 7: ROOT MEAN SQUARED ERROR RMSE OF SIGNIFICANT WAVE HEIGHTS OF WAM COMPARED WITH SATELLITE MEASUREMENTS FROM JASON-1, JASON-2, AND JASON-3. ..... 25

FIGURE 8: BIAS OF SIGNIFICANT WAVE HEIGHTS OF WAM COMPARED WITH SATELLITE MEASUREMENTS FROM JASON-1, JASON-2, AND JASON-3. ..... 25

FIGURE 9: CORRELATION BETWEEN SIGNIFICANT WAVE HEIGHTS OF WAM AND OF SATELLITE MEASUREMENTS FROM JASON-1, JASON-2, AND JASON-3. ..... 26

FIGURE 10: SCATTER INDEX SI DERIVED FROM SIGNIFICANT WAVE HEIGHTS SIMULATED IN WAM AND MEASURED BY THE SATELLITES FROM JASON-1, JASON-2, AND JASON-3. ..... 27

FIGURE 11: REDUCTION OF VARIANCE RV DERIVED FROM SIGNIFICANT WAVE HEIGHTS SIMULATED IN WAM AND FROM COMBINED SATELLITE MEASUREMENTS. ..... 27

FIGURE 12: NUMBER OF VALID SATELLITE OBSERVATIONS FROM JASON-1, JASON-2, AND JASON-3 PER GRID CELL WITHIN THE PERIOD 15.01.2002-02.11.2017. ..... 28

FIGURE 13: ROOT MEAN SQUARED ERROR RMSE OF SIGNIFICANT WAVE HEIGHTS OF WAM COMPARED WITH INDIVIDUAL SATELLITE MEASUREMENTS FROM JASON-1, JASON-2, AND JASON-3. ..... 29

FIGURE 14: BIAS OF SIGNIFICANT WAVE HEIGHTS OF WAM COMPARED WITH INDIVIDUAL SATELLITE MEASUREMENTS FROM JASON-1, JASON-2, AND JASON-3. ..... 30

FIGURE 15: CORRELATION BETWEEN SIGNIFICANT WAVE HEIGHTS OF WAM AND OF SATELLITE MEASUREMENTS FROM JASON-1, JASON-2, AND JASON-3. ..... 31

FIGURE 16: SCATTER INDEX SI DERIVED FROM SIGNIFICANT WAVE HEIGHTS SIMULATED IN WAM AND MEASURED BY THE SATELLITES FROM JASON-1, JASON-2, AND JASON-3. ..... 32

FIGURE 17: REDUCTION OF VARIANCE RV DERIVED FROM SIGNIFICANT WAVE HEIGHTS SIMULATED IN WAM AND FROM INDIVIDUAL SATELLITE MEASUREMENTS. ..... 33

FIGURE 18: AVERAGE SIGNIFICANT WAVE HEIGHT IN WAM CALCULATED OVER THE PERIOD 2002-2017. ..... 34

**FIGURE 19: MAXIMUM SIGNIFICANT WAVE HEIGHT IN WAM CALCULATED OVER THE PERIOD 2002-2017.** ..... 35

**FIGURE 20: STANDARD DEVIATION OF THE SIGNIFICANT WAVE HEIGHT IN WAM CALCULATED OVER THE PERIOD 2002-2017.** ..... 35

**FIGURE 21: AVERAGE MEAN WAVE DIRECTION IN WAM CALCULATED OVER THE PERIOD 2002-2017.** ..... 36

**FIGURE 22: STANDARD DEVIATION OF THE MEAN WAVE DIRECTION IN WAM CALCULATED OVER THE PERIOD 2002-2017.** ..... 36

**FIGURE 23: AVERAGE U-COMPONENT OF THE STOKES DRIFT IN WAM CALCULATED OVER THE PERIOD 2002-2017.** ..... 37

**FIGURE 24: AVERAGE U-COMPONENT OF THE STOKES DRIFT IN WAM CALCULATED OVER THE PERIOD 2002-2017.** ..... 37

**FIGURE 25: AVERAGE STOKES DRIFT IN WAM DERIVED FROM THE AVERAGE OF U- AND V-COMPONENTS (SHOWN IN FIGURE 21 AND 22) CALCULATED OVER THE PERIOD 2002-2017.** ..... 38

**FIGURE 26: EIGENVECTOR OF THE FIRST EMPIRICAL ORTHOGONAL FUNCTION (EOF1). THE EOF1 IS REPRESENTATIVE FOR 61.2 % OF THE VARIANCE.** ..... 38

**FIGURE 27: EIGENVECTOR OF THE SECOND EMPIRICAL ORTHOGONAL FUNCTION (EOF2). THE EOF2 IS REPRESENTATIVE FOR 16.3 % OF THE VARIANCE** ..... 39

**FIGURE 28: EIGENVECTOR OF THE THIRD EMPIRICAL ORTHOGONAL FUNCTION (EOF3). THE EOF3 IS REPRESENTATIVE FOR 6.2 % OF THE VARIANCE.** ..... 39

**FIGURE 29: EIGENVECTOR OF THE FOURTH EMPIRICAL ORTHOGONAL FUNCTION (EOF4). THE EOF4 IS REPRESENTATIVE FOR 4.6 % OF THE VARIANCE.** ..... 40

# LIST OF TABLES


**TABLE 1: EANS FOR THE BLKSEA_REANALYSIS _WAV_007_006 REANALYSIS** ..... 8

# I EXECUTIVE SUMMARY

## I.1 Products covered by this document

This document describes the quality of the multi-year products (MYP) of the wave component of the Black Sea: BLKSEA_REANALYSIS _WAV_007_006. The product includes:

- 2D hourly instantaneous fields of: spectral significant wave height (Hm0), spectral moments (-1.0) wave period (Tm-10), spectral moments (0,2) wave period (Tm02), wave period at spectral peak/peak period (Tp), mean wave direction from (Mdir), wave principal direction at spectral peak, stokes drift U, stokes drift V, spectral significant wind wave height, spectral moments (0,1) wind wave period, mean wind wave direction from, spectral significant primary swell wave height, spectral moments (0,1) primary swell wave period, mean primary swell wave direction from, spectral significant secondary swell wave height, spectral moments (0,1) secondary swell wave period, mean secondary swell wave direction from.

- The output data are produced at 1/27°x1/36° horizontal resolution.

## I.2 Summary of the results

The quality of the MYP BLKSEA_REANALYSIS_WAV_007_006 has been assessed via comparing the reanalyses against satellite observations recorded by the radar altimeters of Jason-1, Jason-2, and Jason-3 for the time period 01/01/2002 to 02/11/2017 and available in-situ observations. The horizontal spatial grid resolution of the BS-waves model is 1/27° in zonal direction, 1/36° in meridional direction (ca. 3 km).

The main results of the BLKSEA_REANALYSIS_WAV_007_006 quality product assessment are summarized below:

**Significant Wave Height**: As the Black Sea lacks buoy data for the time period 2002-2017, all comparisons, except for a short period in 2012 (04-15 February 2012) for significant wave heights have been done with satellite altimeter data. The V4 BS-waves system used to produce BLKSEA_REANALYSIS _WAV_007_006 presents good accuracy in terms of the SWH. The model skill enhancement is evident when considering the different statistical parameters. The skills critically depend upon the quality of the wind forcing for the Black Sea. In total, the wave model results and observations are correlated at a level of 0.86 or better. In general, the wave model tends to underestimate the satellite measurements slightly. The BIAS is always negative with values better than -0.18 m. It is also noteworthy that BLKSEA_REANALYSIS _WAV_007_006 is able to capture the temporal variability very well for almost all parts of the distribution of significant wave heights.

**An important issue for the BS-WAV product validation is the lack of systematic in-situ measurements.**

## I.3 Estimated Accuracy Numbers

Estimated Accuracy Numbers (EANs) for the results of the BS-waves reanalysis are the mean of the differences between measured and computed values “BIAS” and the corresponding RMS error

EANs are computed for:

- Significant Wave Height (SWH): refers to the "spectral significant wave height (Hm0)"

The observations are:

- Significant wave height recorded by the radar altimeters of the satellites Jason-1, Jason-2, and Jason-3 that are available on the public server of AVISO (anonymous@avisoftp.cnes.fr)
- Significant wave height and peak period recorded by the ADCP station Pasha Dere located at 28.03 °E, 43.08 °N

The EANS computed for the V4 version of the CMEMS Black Sea wave modelling system are based on the simulation of the system in hindcast mode for a 16 years-time period between January 2002 and December 2017. With regard to the lack of systematic in-situ measurements in the Black Sea, satellite measurements are the only source to compare the wave model results with. The final values for BIAS and RMSE (common nomenclature of these metrics in the literature of wave modelling) are given in Table 1 for each of the three satellites spanning different periods and for the case when all satellite measurements are combined. Since the BIAS is the difference model mean minus mean of the measurements, the EANs for the BS-waves system indicate an underestimation of the measurements by the wave model.

**Table 1: EANs for the BLKSEA_REANALYSIS _WAV_007_006 reanalysis**

| **2002-2013 (Jason-1)** | | **2008-2016 (Jason-2)** | | **2016-2017 (Jason-3)** | | **2002-2017 (combined)** | |
|---|---|---|---|---|---|---|---|
| BIAS | RMSE | BIAS | RMSE | BIAS | RMSE | BIAS | RMSE |
| -18.1 | 37.1 | -11.5 | 33.7 | -14.0 | 32.0 | -15.4 | 35.4 |

All values in centimetres

# II PRODUCTION SYSTEM DESCRIPTION

## II.1 Production centre details

**PU**: HZG, Germany

**Production chain**: BS-MFC-WAVES

**External product (2D)**: spectral significant wave height (Hm0), spectral moments (-1,0) wave period (Tm-10), spectral moments (0,2) wave period (Tm02), wave period at spectral peak / peak period (Tp), mean wave direction from (Mdir), wave principal direction at spectral peak, stokes drift U, stokes drift V, spectral significant wind wave height, spectral moments (0,1) wind wave period, mean wind wave direction from, spectral significant primary swell wave height, spectral moments (0,1) primary swell wave period, mean primary swell wave direction from, spectral significant secondary swell wave height, spectral moments (0,1) secondary swell wave period, mean secondary swell wave direction from.

**Frequency of model output**: hourly (instantaneous)

**Geographical coverage:** 27.73°E → 41.96°E ; 40.86°N → 46.80°N (the Azov Sea is excluded)

**Horizontal resolution:** 1/27° in zonal direction, 1/36° in meridional direction (ca. 3 km)

**Vertical coverage:** Surface

**Time covered by the reanalysis:** 01 January 2002 to 31 December 2017

The wave reanalysis for the Black Sea is produced by the HZG Production Unit by means of the WAM wave model (described below).

**The BS-waves system integration is composed of several steps :**

1. Upstream Data Acquisition, Pre-Processing and Control of : ECMWF (European Centre for Medium-Range Weather Forecasts) ERA-Interim (atmospheric reanalysis) atmospheric forcing
2. Hindcast/Forecast: WAM produces BLKSEA_REANALYSIS _WAV_007_006.
3. Post processing: the model output is processed in order to obtain the products for the CMEMS catalogue
4. Output delivery

## II.2 System Description

This document details the quality of products from the Black Sea Wave Reanalysis system. These products are generated using a WAM Cycle 4.6.2 3 km Black Sea model, which became operational within CMEMS in April 2017 and was subsequently used to produce the BLKSEA_REANALYSIS _WAV_007_006 reanalysis. The wave model provides a description of ocean surface gravity wave (periods 1.5 to 25 seconds) characteristics as an extension to the existing physical and ecosystem model products provided by the North-West Shelf MFC. The following subsections describe the model component and its dependencies in terms of models providing the forcing.

### Region, grid and bathymetry

The regional wave model for the semi-enclosed Black Sea runs in shallow water mode on a model grid situated between 40°51'36" N to 046°48'16" N and 27°22'12" E to 41°57'45" E, with a spatial resolution of about 3 km, also 100 seconds in latitude, respectively 133 seconds in longitude. The required bathymetry for the model grid bases upon the General Bathymetric Chart of the Oceans (GEBCO, http://www.gebco.net) 1-arc minute data. The bathymetry is only a controlling mechanism on the wave field for depths below approximately 490 m, based on a minimum frequency in the model of approximately 0.04 Hz (period 25 seconds). The model area and the corresponding depth distribution are shown in figure 1.

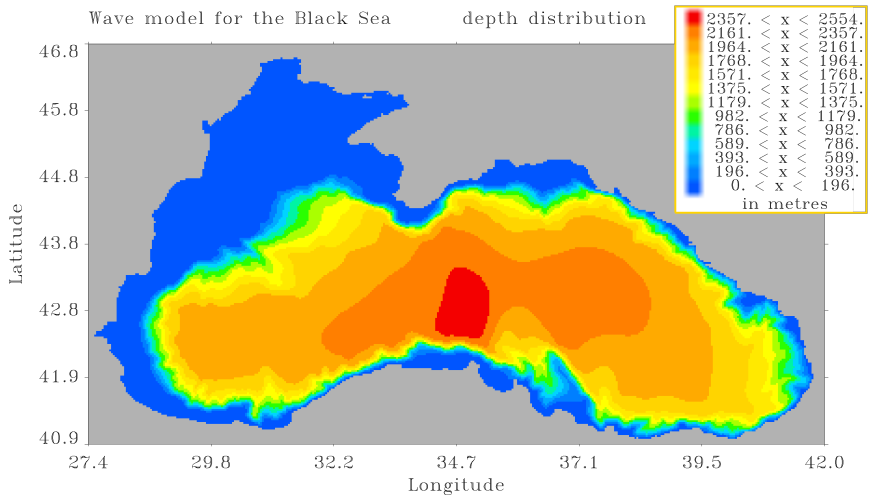


**Figure 1: Black Sea Wave model WAM depth distribution**

### Spectral grid

WAM calculates the two-dimensional energy density spectrum at each of the 44699 active model grid points in the frequency and directional space. The solution of the energy balance equation is provided for 24 directional bands at 15° each, starting at 7.5° and measured clockwise with respect to true

north, and 30 frequencies logarithmically spaced from 0.042 Hz to 0.66 Hz at intervals of Δf/f = 0.1. Therefore the prognostic part of the wave model covers periods from approximately 25 to 1.5 seconds. In order to include the important contribution of higher frequency waves to wave growth/dissipation processes and the output wave characteristics a parametric tail is fitted for frequencies above the spectral maximum (e.g. WAMDIG, 1988)

**Wave model and source term physics configuration**

The system BS-waves is based on the state-of-the-art and well-established advanced third generation spectral wave model WAM that runs successfully at many institutions worldwide. It is based on the spectral description of the wave conditions in frequency and directional space at each of the active model sea grid points of a certain model area. The energy balance equation, complemented with a suitable description of the relevant physical processes is used to follow the evolution of each wave spectral component. WAM computes the two dimensional wave variance spectrum through integration of the transport equation (1) in spherical coordinates:

$$\frac{\partial F}{\partial t} + (\cos\Phi)^{-1}\frac{\partial}{\partial \Phi}(\dot{\Phi}\cos\Phi \mathrm{F}) + \frac{\partial}{\partial \lambda}(\dot{\lambda}F) + \sigma\frac{\partial}{\partial \sigma}\left(\dot{\sigma}\frac{F}{\sigma}\right) + \frac{\partial}{\partial \theta}(\dot{\theta}F) = S$$

with

$\mathrm{F}(\lambda, \Phi, \sigma, \theta, \mathrm{t})$

$\dot{\Phi} = (c_g \cos\theta + u_{North})/R$

$\dot{\lambda} = (c_g \sin\theta + u_{East})/(R\cos\Phi)$

$\dot{\theta} = c_g \sin\theta \tan\Phi/\mathrm{R} + \dot{\theta}_D + \dot{\theta}_C$

$\dot{\sigma} = \dot{\sigma_C}$

wave energy density spectrum

$(\lambda, \phi)$ longitude, latitude

$(\sigma, \theta)$ intrinsic frequency, wave direction

The first term of (1) describes the local rate of change of energy density in time, the second and third ones the propagation in geographical space, the fourth one the shifting of the relative frequency due to variations in depths and currents and the last one on the left side of the equation the contribution of the depth- and current-induced refraction. The source functions on the right of the transport equation comprise the contributions of wind input ($S_{in}$), nonlinear interaction ($S_{nl}$), dissipation ($S_{dis}$), bottom friction ($S_{bf}$) and wave breaking ($S_{br}$):

$S = S_{in} + S_{nl} + S_{ds} + S_{bf} + S_{br}$

A detailed description is given by the WAMDI group (1988), Komen et al. (1994), Günther et al. (1992) and Janssen (2008). The WAM Cycle 4.5.4 that is used for the Black Sea wave hindcast is an update of the former WAM Cycle 4. The basic physics and numerics are kept in that new release. The source function integration scheme made by Hersbach and Janssen (1999), and the model updates by Bidlot et al. (2007) are incorporated. The wave model performance has been discussed in Staneva at al., (2015, Behrens, 2014, Staneva et al. 2016a,b,c)

Time dependent depth and current fields as well as assimilation of measurements into the wave fields is not used in this setup whereas wave breaking has been taken into account. The wave model WAM is not coupled to a hydrodynamic model in this application.

**Forcing**

The driving forces for the wave model are the $U_{10}$ wind fields provided by the atmospheric reanalysis ERA-Interim of the ECMWF (European Centre for Medium-Range Weather Forecasts) via the CMCC server. The temporal resolution of the wind forcing is 6-h for the hindcast. The native spatial resolution ERA-Interim is about 0.71 degrees horizontally.
Boundary values are not considered as the Black Sea is a semi enclosed area.

**Wave growth**

In order to reduce possible underestimates of satellite radar altimeter measurements by the wave model, the parameterisation of the wave growth in the wind input source term has been adapted to the driving wind fields. The source term for the wind input is :

$$S_{in} = \gamma F \qquad \text{(wave growths rate} * \text{spectrum)}$$

The growth rate, normalised by the angular frequency ω, derived from a parametrization by Peter Janssen (1991) results from :

$$\frac{\gamma}{\omega} = \varepsilon \beta x^2$$

$\varepsilon$ : air water density ratio
$\beta$ : Miles parameter
$x = (\frac{u*}{c}) \max(\cos(\theta - \varphi), 0)$

The Miles parameter β depends again on a constant called $\beta_m$ with a value of 1.2 after Peter Janssen (1991), but has been adapted to $\beta_m$ = 1.5 for the Black Sea in order to enable stronger wave growth.

**Partitioning method**

Included in model outputs are characteristics describing individual wave components that make up a given sea-state. For example, a sea may consist simply of a single wind-sea component for which all wave energy is affected by the forcing wind, or multiple swell components which have been remotely

generated by distant storms. In WAM these components are determined using a two stage process. Individual components are derived from the two dimensional wave spectrum. This process effectively treats the wave spectrum as a topographic map from which individual peaks in wave energy can be identified in order to define the separate wave components.

The second part of the procedure follows an assumption that wind sea should be defined as only that part of the wave energy spectrum which is directly forced by the wind (this is an assumption which is most regularly used by operational wave forecasters who wish to be able to reference the evolution of wind sea directly against evolution in the local wind conditions). Using this assumption, wave spectrum bins where wave speed is slower than the (co-directed) wind speed are associated with the wind sea component. The assignment of spatial energy to wind sea overrides any previous assignment of wave energy to the topographic components made in the first step.

# III VALIDATION FRAMEWORK

The quality of the skill and temporal variability of the 16 years long reanalysis BLKSEA_REANALYSIS _WAV_007_006 spanning the period 01 January 2002 to 31 December 2017 is assessed by comparing the simulated significant wave heights with measurements provided by a set of satellites, namely Jason-1, Jason-2, and Jason-3 covering most of reanalysis period. For the comparison, we match significant wave heights from the satellites and BLKSEA_REANALYSIS _WAV_007_006 in time and space.

## III.1 Quality control of the satellite data

Before making use of the satellites, the data need filtering to ensure physically plausible significant wave heights. Even though the data provided by Aviso (https://www.aviso.altimetry.fr) had been quality controlled, we found several cases that warranted further verification. Our quality control comprises manual and automatic filtering. At first, we screen the data to find obviously incorrect measurements, from which we derive criteria for automatic filtering. For instance, we remove all measurements, where the measured significant wave height equals 0. We also remove outliers that would possibly compromise our analysis. We define outliers as values farther away than 2 standard deviations from the linear slope-fit between measured and modelled data.

## III.2 Statistical analysis

We present scatter plots that show measured against modelled significant wave heights for each of the satellites separately. We also consider the case, for which all the measurements are combined without distinguishing between satellites.

We illustrate overplotting (as there are hundreds of thousands pairs of measured and modelled data) by estimating the bivariate probability density through evaluating a 2d-gaussian kernel on a square grid in the variable space (Venables and Ripley, 2002). The size of the grid cells is in the order of $10^{-5}$ $m^2$.

Furthermore, the plots include summary statistics, such as the mean value and standard deviation, and statistics that describe the skill of WAM to simulate the significant wave heights for the whole period. The reanalysis spans the period 01.01.2002 to 31.12.2017, which also includes numerous measurements from the newly started Jason-3 mission (up to 02.11.2017 as of writing).

The skill scores used are Pearson's product-moment correlation coefficient, the root mean squared error RMSE, the bias, the scatter index SI (e.g. Chawla et al., 2013), and the reduction of variance RV. The scores read as follows, where o and m stand for observed and modelled data. An overbar over a variable denotes the average value derived from the sample of length n.

$$Correlation = \frac{\frac{1}{n-1}\sum_{i=1}^{n}(o_i - \bar{o})(m_i - \bar{m})}{\sqrt{\frac{1}{n-1}\sum_{i=1}^{n}(o_i - \bar{o})^2}\sqrt{\frac{1}{n-1}\sum_{i=1}^{n}(m_i - \bar{m})^2}}$$

$$RMSE = \sqrt{\frac{1}{n}\sum_{i=1}^{n}(m_i - o_i)^2}$$

$$BIAS = \frac{1}{n}\sum_{i=1}^{n}(m_i - o_i)$$

$$SI = \frac{\sqrt{\frac{1}{n-1}\sum_{i=1}^{n}(m_i - o_i - BIAS)^2}}{\bar{o}}$$

$$RV = 1 - \frac{\sum_{i=1}^{n}(m_i - o_i)^2}{\sum_{i=1}^{n}(o_i - \bar{o})^2}$$

One of the general assumptions for the correlation coefficient is that variables follow a normal distribution, which is not the case for the significant wave height. It might be advisable to use another measure to gauge the monotonic relation between modelled and observed significant wave heights, such as the rank correlation. However, we use Pearson's correlation coefficient as it is a quasi-standard for evaluating numerical models.

The scatter plots also show the least-squares linear fit without including any intercept between measurements and modelling results. Ideally, such a fit would be close to the straight line dividing the scatter plot at an angle of 45°, which is included as a reference.

Last, we also show pairs of quantiles of the measured and modelled significant wave heights. The quantiles are estimated from the empirical cumulative density function at specific percentiles 0.4 % apart from each other. The highest quantile shown corresponds to the sampled maximum value, which translates to the 100$^{th}$ percentile of the empirical distribution.

### III.3 Time series analysis

The length of the combined satellite measurements allows further assessing the quality of the dataset through computing time series of statistical properties, which are derived on shorter time scales. We assume that already monthly intervals would contain enough information to represent the Black Sea properly, but increasing time scales further improves the informational content. Short time scales are potentially affected by the data availability of the satellites: The duration of one satellite passing over the Black Sea lasts for minutes only. Fly-overs happen once to twice daily. Consequently, very short statistics, e.g. on the daily scale, would not represent the Black Sea waves adequately. Therefore, we have chosen to use the annual scale in the following.

We compute time series of specific quantiles, mean, minimum, and maximum values of measured significant wave heights for each year in the measurement period of the satellites. We apply this procedure to the corresponding simulated significant wave heights from WAM for a comparison. The quantiles have been selected to represent the whole distribution of significant wave heights with a

focus on the upper quantiles. Similar to the scatter plots we provide the correlation, bias, and RMSE, but also include the relative error, which reads

$$RE = \frac{\frac{1}{n}\sum_{i=1}^{n}(m_i - o_i)}{\bar{o}}$$

Note that this method heavily depends on the location and time of the satellite tracks and cycles. It is very likely that our approach does not catch all notable wave events. However, by using a relatively long interval to aggregate statistics, we can assume that our statistics are robust and, as a time series, can represent the wave climate of the Black Sea.

In principle, using this method would also allow to create a gridded dataset in a relatively coarse resolution. However, creating a gridded dataset has the drawback of only being statistically robust on the grid point level when the time intervals and grid cell sizes used are big enough to collect a sample large enough.

### III.4 Spatial statistics

To complement our analyses, we also provide figures showing the aforementioned statistics along the satellite tracks. Note that Jason-1 had technical difficulties in 2012, after which Jason-1 transitioned to its interleaved orbit (e.g. https://www.aviso.altimetry.fr/en/missions/past-missions/jason-1/orbit.html). Shortly afterwards, the satellite mission ended. Interestingly, Jason-1 continued its measurements during this period. After carefully checking the values in 2012, we decided to utilize them as they passed our own quality check.

# IV VALIDATION RESULTS

## IV.1 Statistical analysis

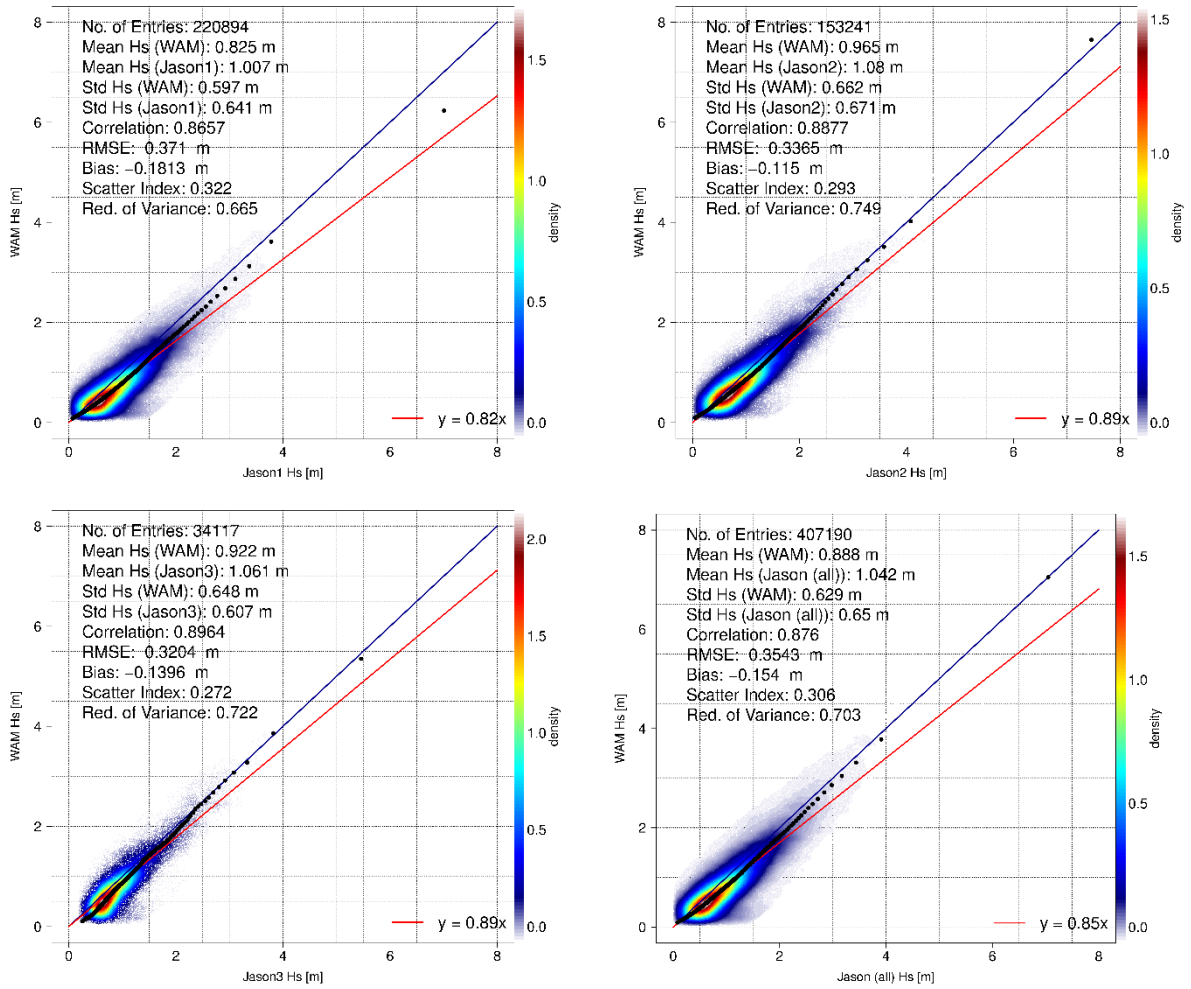


**Figure 2: Scatter plots showing satellite measurements versus modelled significant wave heights for the periods 15.01.2002-20.06.2013 (Jason-1), 04.07.2008-15.07.2017 (Jason-2), 13.02.2016-02.11.2017 (Jason-3), and 15.01.2002-02.11.2017 (all satellites merged). Also shown are the estimated bivariate probability density, the linear slope-fit regression of modelled and observed wave heights, and specific quantiles taken from the empirical cumulative density function. Furthermore, summary statistics and skill scores are included.**

Making use of the measurements from 3 different satellite missions gives the chance to assess how well WAM can simulate past significant wave heights within the Black Sea. Figures 2 depicts the scatter plots for the comparison between modelled significant wave heights and the satellites (Jason-1, Jason-2, Jason-3 and the combination thereof). In general, most of the values are located between 0.8 to 0.9 m for WAM and 1.0 to 1.1 m for the satellites, already hinting at an underestimation of the wave heights in WAM. The calculated biases of WAM for the different satellites confirm the underestimate

being in the range of -0.12 m (Jason-2) to -0.18 m (Jason-1). This bias, which describes the average error of the simulations, is also visible in Figure 2, where matched pairs of quantiles of simulated and observed values and the linear regression deviate from the 45°-line downwards. The RMSE, on which the bias has strong influence and which represents the magnitude of model errors, varies from 0.32 m (Jason-3) to 0.37 m (Jason-1). Another source of the deviations lies in the difference of the simulated and modelled variability, here given as the standard deviations. The differences range from about 1 cm (Jason-2) to 4 cm (Jason-1). Note that measurement errors and noise that our initial quality control has not filtered out can also impair the RMSE and the standard deviation of the measurements, thus potentially degrading the model skill. Additionally, the wind fields also influence the model variability and skill as they force the wind-wave model WAM. The forcing fields reflect real atmospheric winds only to a certain extent regarding magnitude and variability as they come from the spatially coarse 6-hourly ERA-Interim reanalysis.

However, contrary to these deficiencies, the correlation, as a measure for how well the wave heights of WAM and of the satellites are positively linearly related, is in the range of 0.87 to 0.90 showing a strong linear relationship. Furthermore, the scatter index SI and the reduction of variance score RV support the skilfulness of WAM as they are relatively low (high) with values between 0.27 (0.72) for Jason-3 to 0.32 (0.66) for Jason-1. Both skill scores benefit from the high correlations as the correlation counteracts the influence of the bias and the RMSE in SI and RV. Note that in comparison with skill assessments from short-term wave analyses and forecasts (see QUID report for BLKSEA_ANALYSIS_FORECAST_WAVES_007_003 for instance), the overall skill of the long reanalysis product is slightly lower due to the long period examined, in which systematic biases, measurement errors and noise can accumulate.

### IV.2 Comparison with Pasha Dere

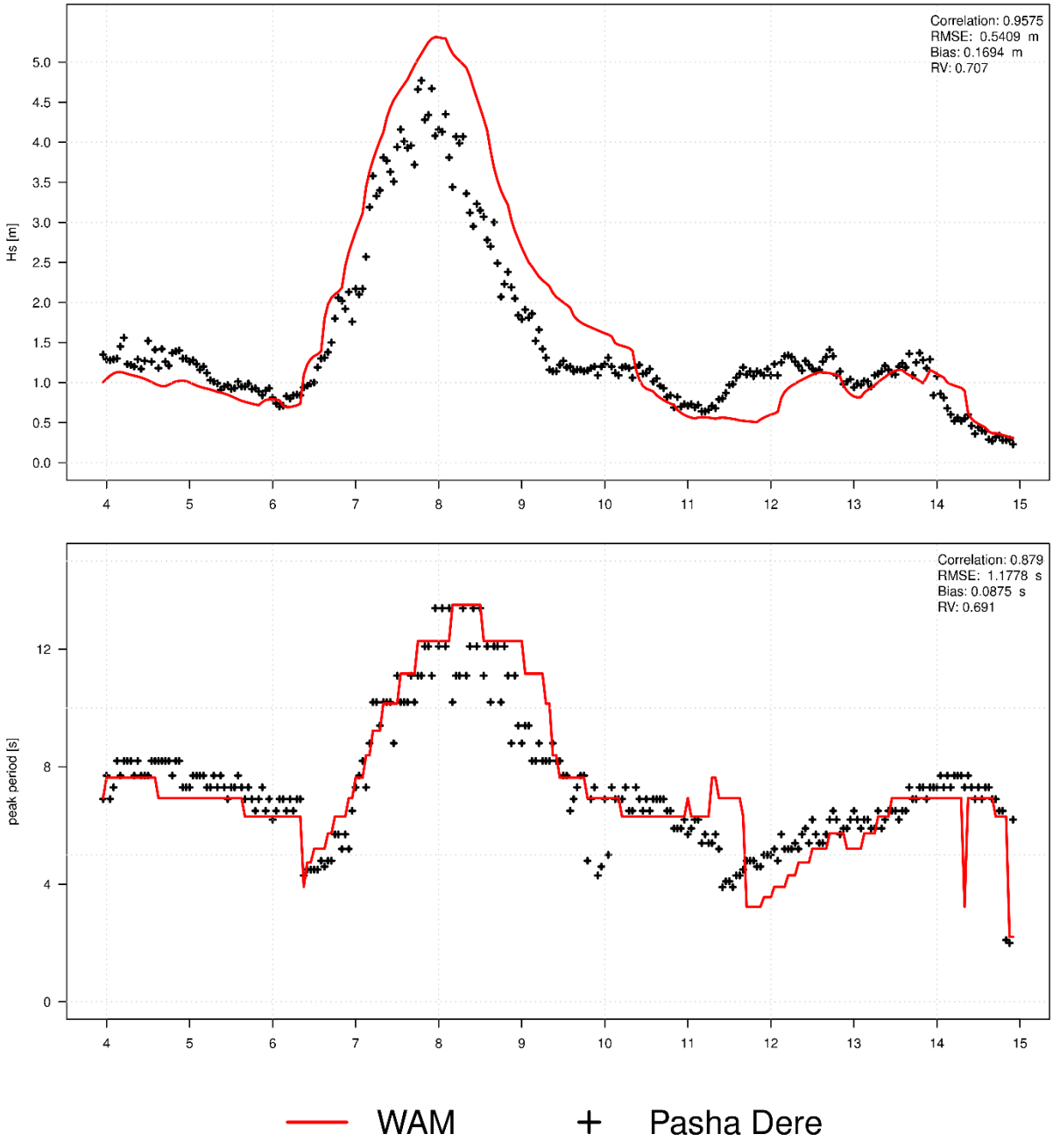


**Figure 3: Significant wave height and peak period from WAM and from the ADCP station Pasha Dere in the period 04-15 February 2012.**

For a short time period of 11 days between 04 February 2012 to 15 February 2012, ADCP data at the location Pasha Dere (located at 28.03 °E, 43.08 °N) in the western part of the Black Sea near the Bulgarian coast was available. The comparison with WAM for the significant wave height and peak

period is shown in Figure 3. The measured and modelled time series of the significant wave height and peak period show good agreement. The skill scores given support the findings. The bias for the significant wave height is about 17 cm, the RMSE 54 cm. The correlation and reduction of variance scores are very high with values of about 0.96 and 0.71.

## IV.3 Time series analysis


**Figure 4: Time series of annual minimum, mean, and maximum significant wave heights, as well as time series of specific annual quantiles of significant wave heights derived from Jason satellite measurements and from WAM.**

Time series of wave statistics derived from satellites and WAM give the chance to examine the temporal variability of specific parts of the wave height distribution and allow further assessing the skill of WAM.

As shown in Figure 4, the mean annual wave heights increase from around 0.8 m to 1.1 m from 2002 to 2016 in WAM, and from about 1.0 m to 1.2 m in the satellite measurements, whereby WAM consistently shows an underestimation, which is reflected in a negative bias of about 15.3 cm. However, the mean annual wave height of WAM and from satellite measurements are highly correlated. At a correlation of about 0.908, the variability of the model and of satellite measurements agree very well with each other. On the contrary, minimum annual wave heights do not exhibit such an agreement. The correlation is 0.03 indicating no skill. As the satellites do not measure very low wave heights accurately, low wave height measurements are prone to errors, which even the initial quality control cannot filter out.

The annual maximum significant wave heights derived from satellite measurements and from WAM show a correlation of about 0.83, which demonstrates that WAM can simulate the temporal variability of maximum wave heights well. Furthermore, WAM underestimates the maximum wave height resulting in a negative bias of 44.2 cm (translating to a relative error of -7.81 %). There are two years, namely 2004 and 2016, for which the maximum significant wave heights match very well. 2004, for instance, was a year, in which the number of storm events was exceptionally high (see Fig. 26 in Arkhipkin et al., 2014). The years in between 2004 and 2016 are characterized by underestimates of the maximum wave heights in WAM.

The annual quantiles of significant wave heights from the 25$^{th}$ to the 99$^{th}$ percentiles representing almost three quarter of the distribution show a temporal behaviour similar to that of the annual mean significant wave height. With higher percentiles considered, the annual variability increases. The correlation ranges between 0.86-0.95 and demonstrates very good skill in catching the variability of wave heights in the Black Sea. Even though the absolute bias increases for increasing quantiles, the relative error decreases to -3.97 % for the annual 99$^{th}$ percentile. The skill of WAM thus increases with higher percentiles, which possibly relates to parametrizations within WAM that slightly degrade the skill for smaller wave heights in favour of larger waves. It is interesting to note that the peaks seen before in the years 2004 and 2016 are not as present as in the annual maximum significant wave heights.

Making use of the annual time scale provides enough samples to examine quantiles even higher than the 99$^{th}$ percentile and helps to understand the peak values in 2004 and 2016 with respect to transitioning from the lower parts of the distribution to the uppermost part. Figure 5 shows the time time series of the annual 99$^{th}$, 99.9$^{th}$, and 99.99$^{th}$ percentiles of significant wave heights.

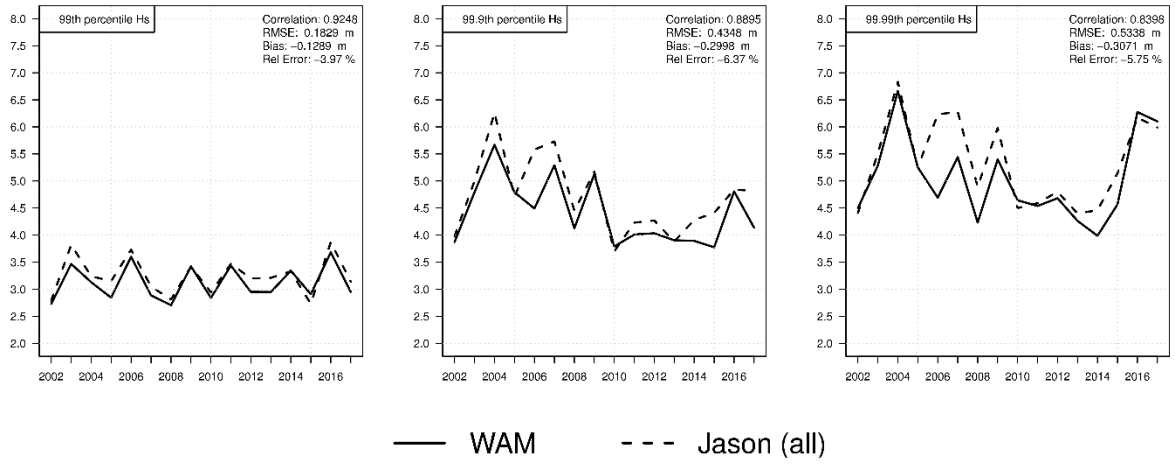


**Figure 5: Upper annual quantiles of significant wave heights derived from satellite measurements and WAM.**

While the annual 99$^{th}$ percentiles show a variability evenly distributed over the whole period with a very good agreement in the time series behaviour, the 99.9$^{th}$ and 99.99$^{th}$ percentiles in WAM become dominated by the peaks in 2004 and 2016, while the values in between deviate further from the satellite measurements without matching the magnitude of the variability. This leads to a slightly degraded skill for the 99.99$^{th}$ percentiles. These very high percentiles represent only a very small number of observations attributable to single events that do not affect lower quantiles of the distribution markedly.

Several factors might hamper the assessment of significant wave heights. First, the wind-wave model WAM, for which simulated wave heights depend on the wind forcing to a large extent, needs wind fields that include high wind speeds at the right time and space to model wave heights in agreement with satellite observations. Here, the used wind fields are taken from the ERA Interim reanalysis, which provides data in a 6-hourly 0.75°x0.75° resolution. It is very likely that elevated wind speeds that cause very high significant wave heights, as seen from the satellites, are not present in the forcing wind fields possibly explaining the deviations in between 2004 and 2016 for the uppermost percentiles and maximum wave heights. In 2004, a year with an exceptional high number of storm events (see Arkhipkin et al., 2014) over the Black Sea, ERA Interim likely includes wind speeds lasting long enough at the right time and at the right location to let WAM-wave heights match observed wave heights. Second, satellites measure wave heights along tracks in a very fine temporal and spatial resolution that is much more detailed than the simulated wave fields of WAM. In our analysis, we match satellite measurements with their closest match in WAM introducing a sampling error that affects all parts of the wave distribution in our analysis.

## IV.4 Spatial statistics

Here, we present the statistics calculated for the scatter plots along the satellite tracks of all combined satellite missions to include as many samples as possible. Plots for the single satellites are given in section IV.4.1

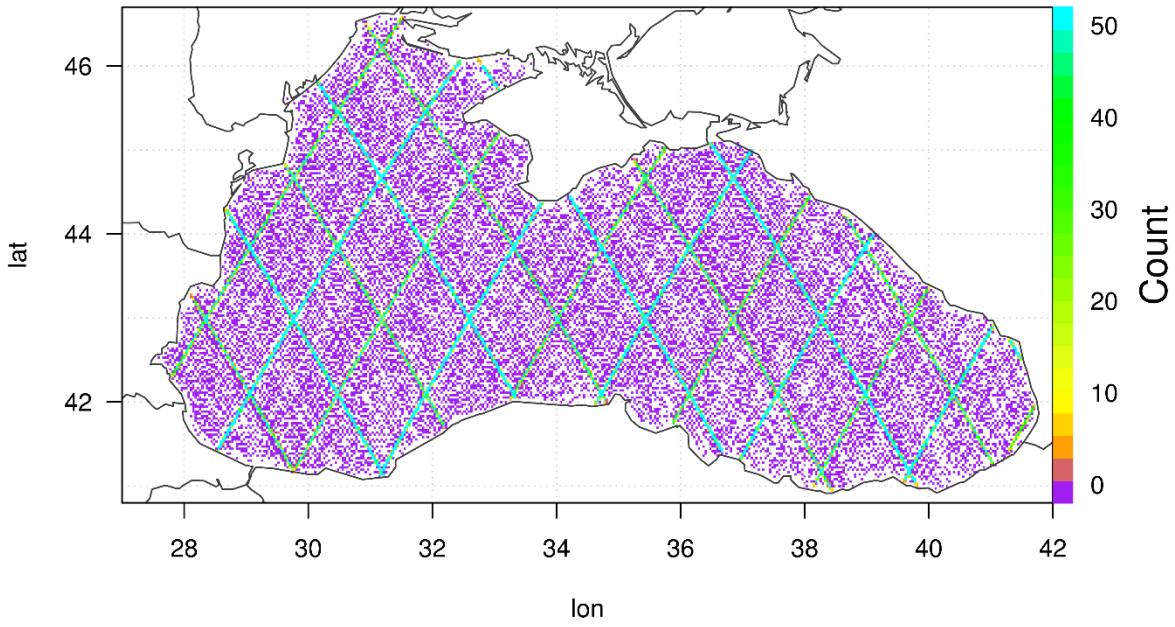


**Figure 6: Number of valid combined satellite observations from Jason-1, Jason-2, and Jason-3 per grid cell within the period 15.01.2002-02.11.2017.**

Figure 6 shows the number of valid satellite measurements per grid cell combined for all three satellite missions. There are three things noteworthy here. First, huge areas of the Black Sea are covered with grid cells containing less than two observations. These observations can be traced back to the last year of Jason-1 measurements, when Jason-1 was gradually shifted towards an interleaved orbit shifted by 1 degree and eventually went out of service in 2013 (see https://arstechnica.com/science/2013/07/last-transmitter-dies-finalizing-retirement-for-ocean-sensing-satellite/ and https://www.aviso.altimetry.fr). However, Jason-1 kept taking measurements during its transition that proved valid in our initial quality check. Second, tracks with a very high number of measurements (more than 50 for each grid cell) are set 2 degrees apart from each other corresponding to the official description of the Jason-satellite missions (see, for instance, https://www.aviso.altimetry.fr). Third, the interleaved orbits of both Jason-1 and Jason-2 before they went out of service are shifted 1 degree away from their nominal orbits (see https://www.aviso.altimetry.fr/en/missions/past-missions/jason-1/orbit.html and https://www.aviso.altimetry.fr/en/missions/current-missions/jason-2/orbit.html), but still provide between 20 to 30 valid measurements per grid cell.

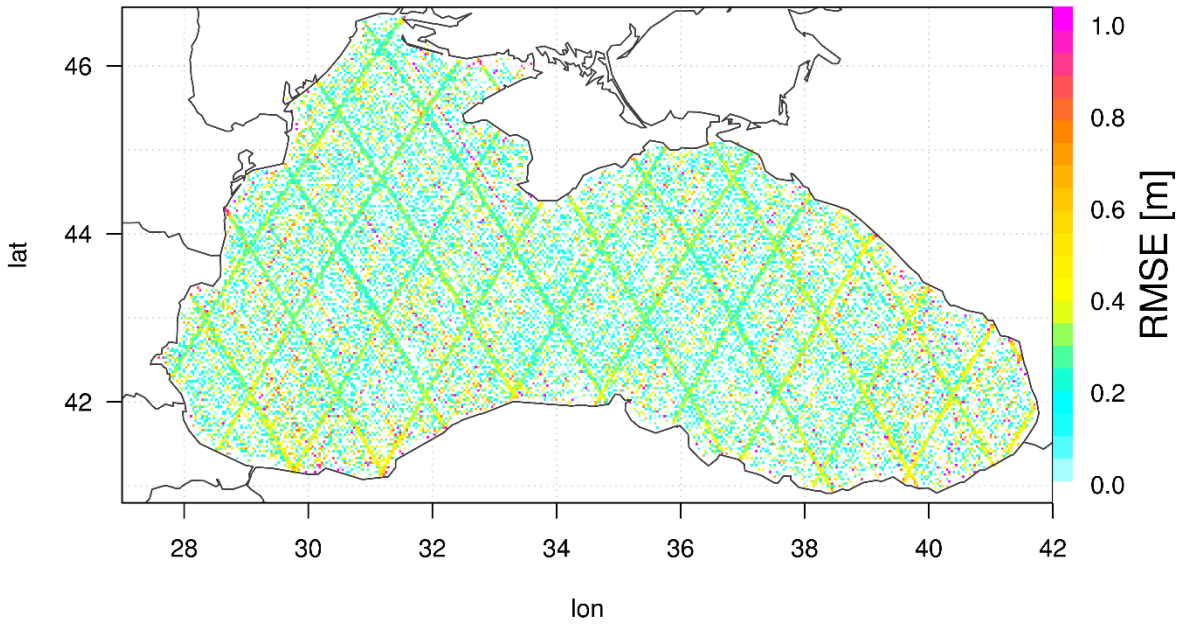


**Figure 7: Root mean squared error RMSE of significant wave heights of WAM compared with satellite measurements from Jason-1, Jason-2, and Jason-3.**

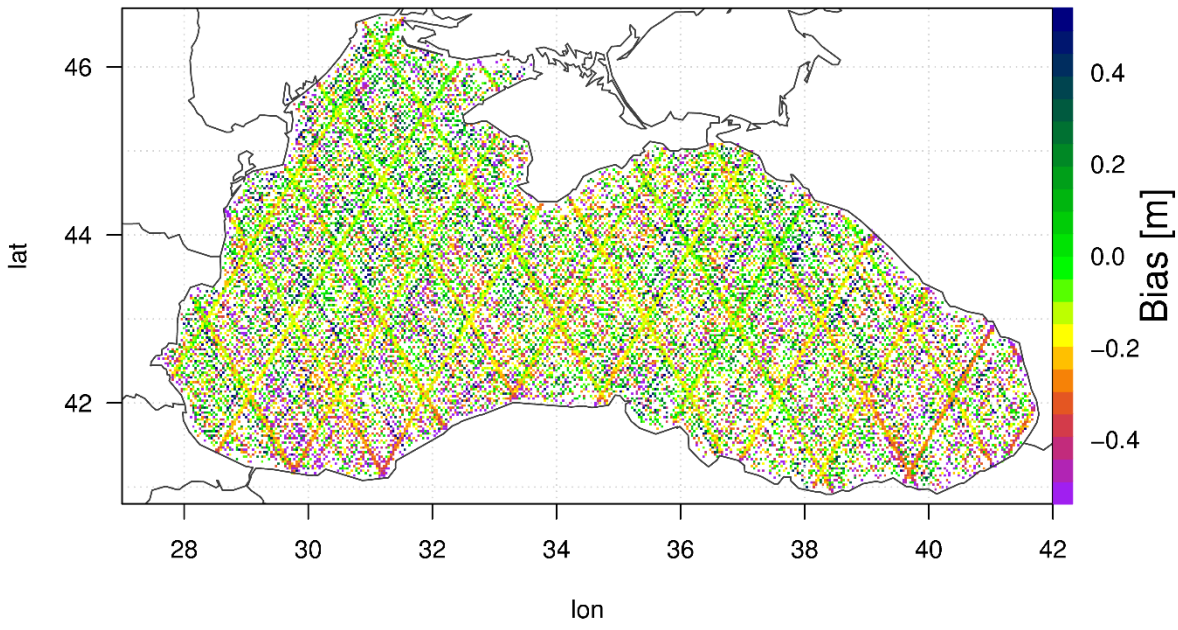


**Figure 8: Bias of significant wave heights of WAM compared with satellite measurements from Jason-1, Jason-2, and Jason-3.**

Error measurements are shown in Figures 7 and 8. While the RMSE is mostly below 0.36, higher values of up to 0.6 are often obtained near coasts, for instance in the southwest. Moreover, the whole area is scattered with single grid cells showing RMSEs above 0.8 m attributable to measurements taken by

Jason-1 during its transition to its interleaved orbit. Overall, the bias confirms the results obtained through the RMSE, but also reveals that near-coastal areas, such as in the southwest or southeast, suffer from underestimated wave heights in WAM, whereas single randomly scattered grid cells in the domain of the Black Sea denote an overestimation. Near-coastal areas are regions, where the precision of satellite measurements is degraded by the rapid transition between land and sea surfaces. Furthermore, for these areas the wave model not only needs a detailed bottom topography, but also needs physical parametrizations suitable for near-coastal wave effects. Thus, degraded error measurements in near-coastal areas may be a combined effect of both the quality of the satellite measurements and the wave model itself.

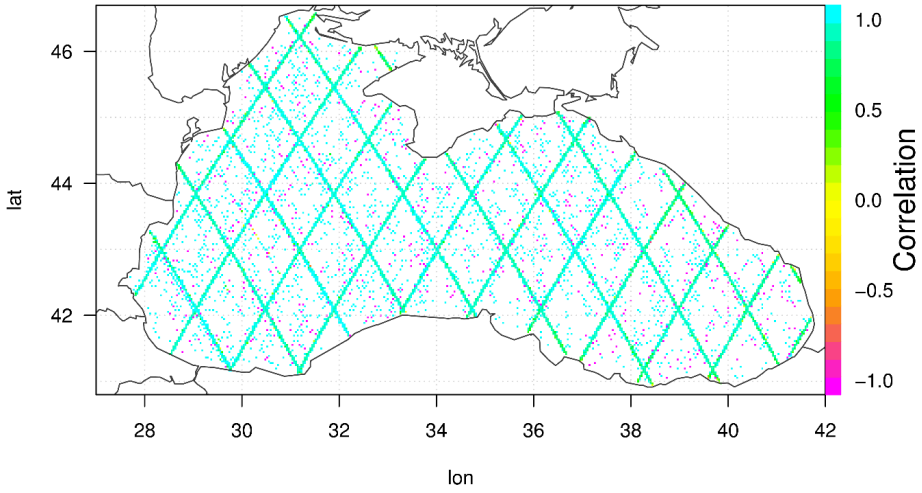


**Figure 9: Correlation between significant wave heights of WAM and of satellite measurements from Jason-1, Jason-2, and Jason-3.**

The correlation, as shown in Figure 9, confirms the findings for the univariate assessment above. The correlations are high in the open sea with values between 0.9 and 1 in the open sea. Slightly less correlations can be found at near-coastal areas, for instance in the north and the east, where the values range around 0.5. The correlation is also calculated in between tracks, where enough measurements are available. However, many single randomly scattered points show a large negative correlation most likely connected to the small of number of measurements taken at these locations.

The scatter index shown in Figure 10 ranges between 0.2 and 0.4 for most of the grid cells within the model domain agreeing with the univariate scatter index, which is about 0.3. There are some grid cells scattered randomly with high SI values between 0.8 and 1.0 that appear in the areas where the transitioning of Jason-1 to its interleaved orbit took place.

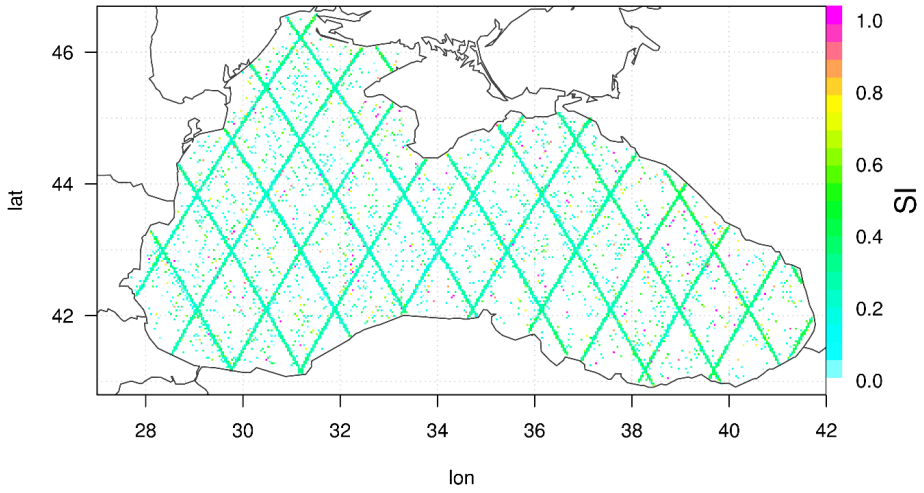


**Figure 10:** ***Scatter index SI derived from significant wave heights simulated in WAM and measured by the satellites from Jason-1, Jason-2, and Jason-3.***

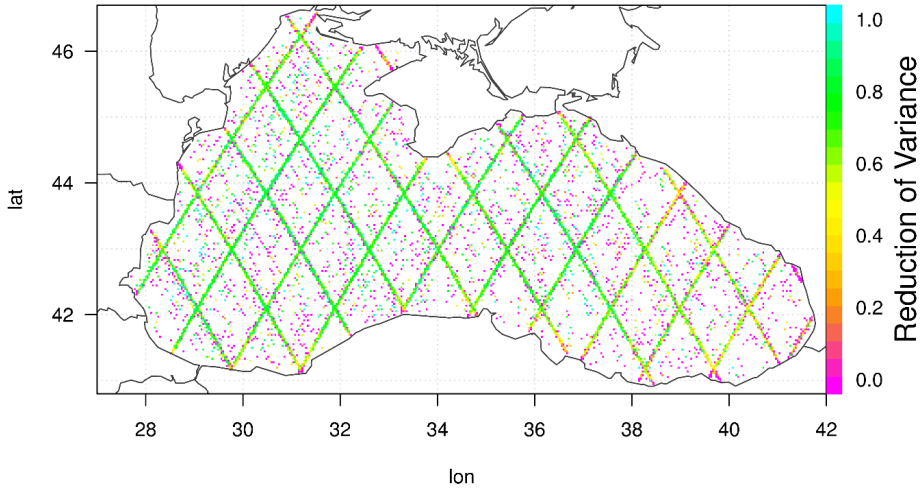


**Figure 11: Reduction of Variance RV derived from significant wave heights simulated in WAM and from combined satellite measurements.**

Finally, Figure 11 depicts the reduction of variance RV. It confirms the previous findings combined in one measure of skill. It demonstrates that along tracks in the open sea, where the number of observations is high, WAM agrees very well with satellite observations with RV values between 0.6 and 0.8. Over near-coastal areas, the skill degrades notably to values slightly above 0. Furthermore, single grid cells randomly scattered all over the Black Sea bear no skill due to the reduced number of observations available, which put biases and observations into the same order of magnitude and consequently degrade the skill to 0 in such places.

Spatial statistics of the individual comparison of WAM and the satellites

To complement the previous analyses the following figures (Figures 12-17) depict the spatial statistics for each of the satellites individually.

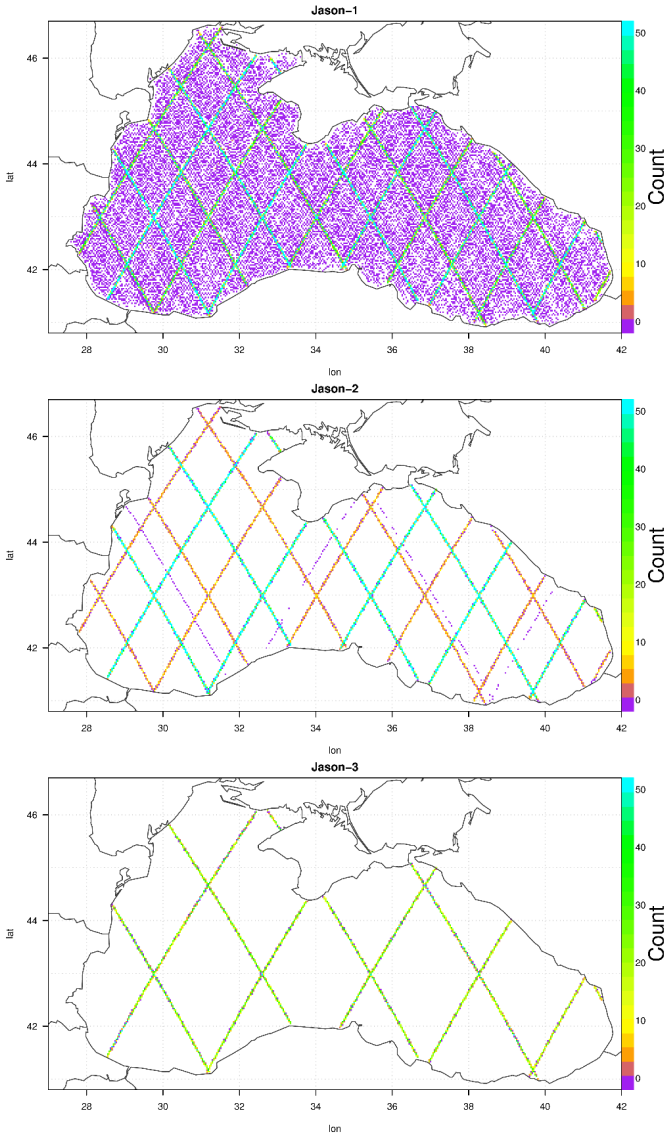


**Figure 12: Number of valid satellite observations from Jason-1, Jason-2, and Jason-3 per grid cell within the period 15.01.2002-02.11.2017.**

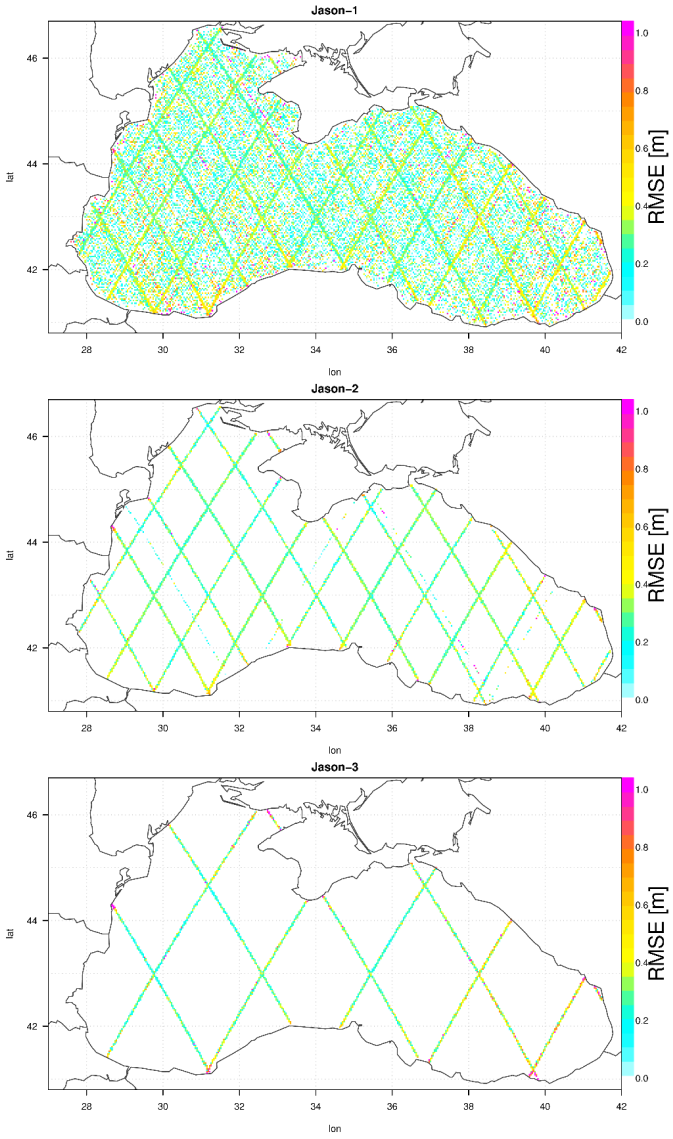


**Figure 13: Root mean squared error RMSE of significant wave heights of WAM compared with individual satellite measurements from Jason-1, Jason-2, and Jason-3.**

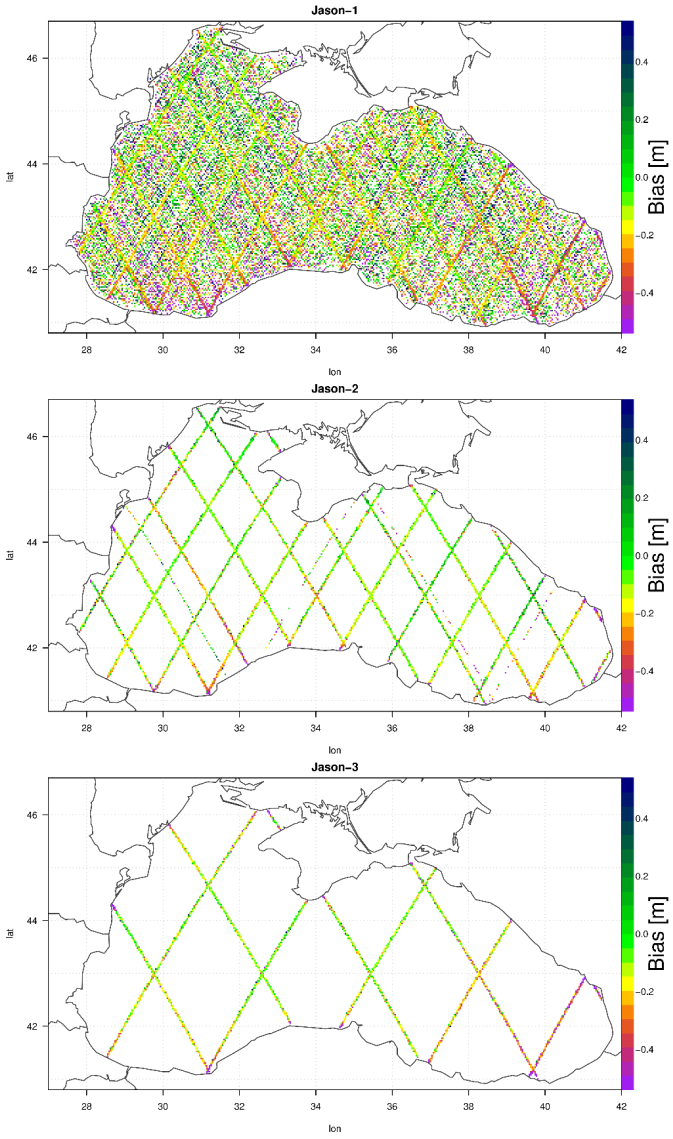


**Figure 14: Bias of significant wave heights of WAM compared with individual satellite measurements from Jason-1, Jason-2, and Jason-3.**

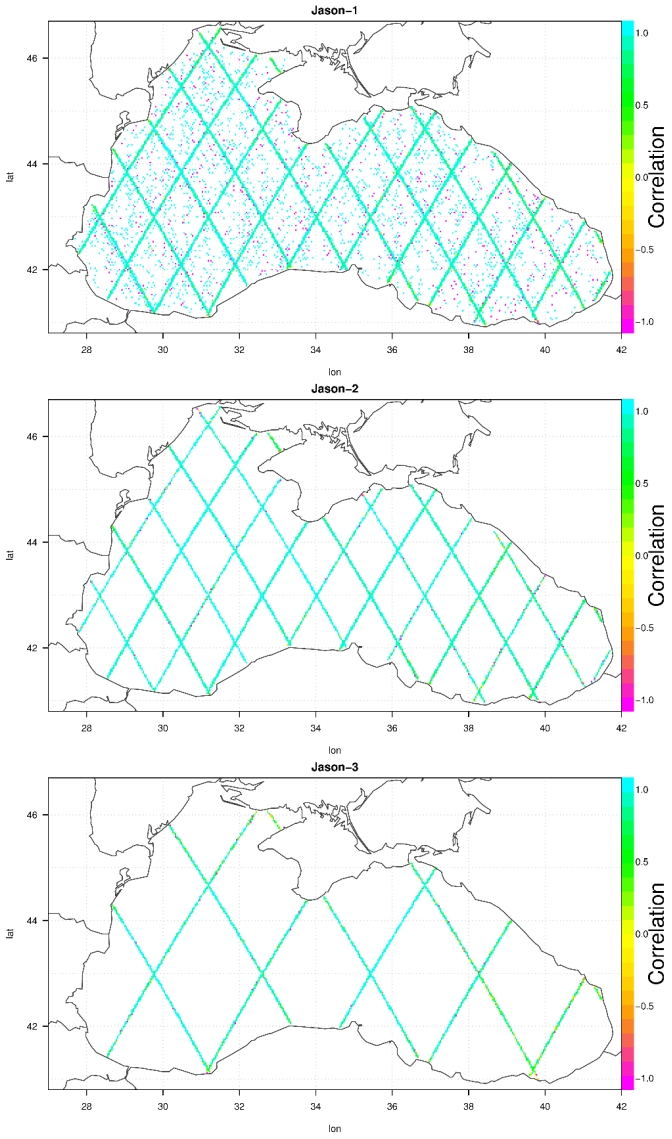


**Figure 15: Correlation between significant wave heights of WAM and of satellite measurements from Jason-1, Jason-2, and Jason-3.**

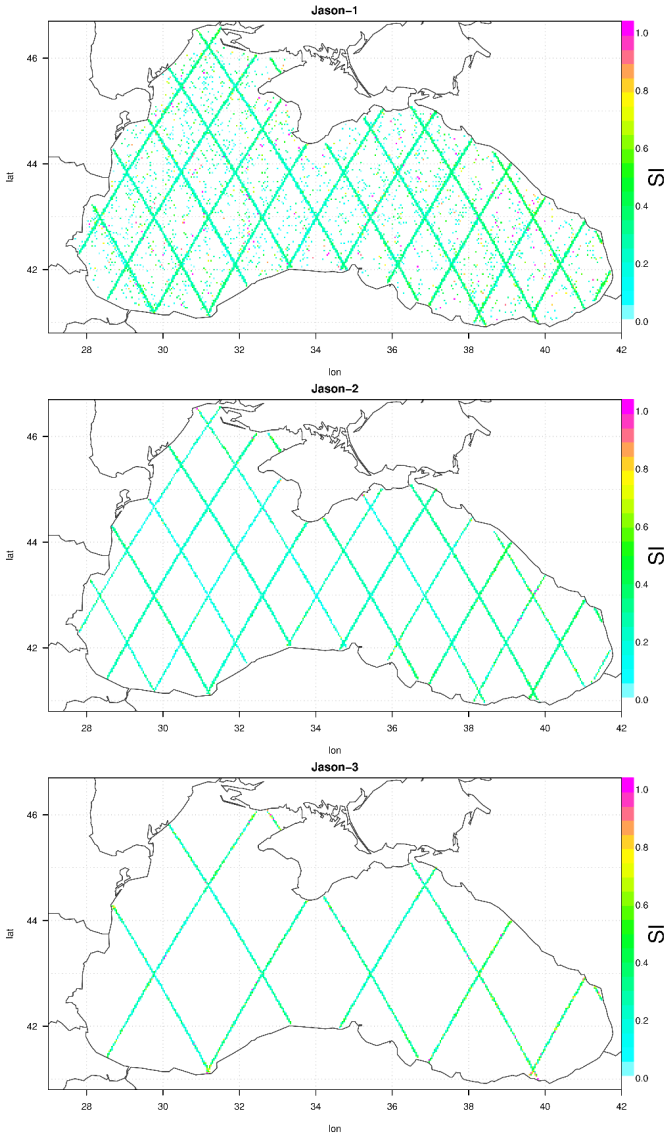


**Figure 16: Scatter index SI derived from significant wave heights simulated in WAM and measured by the satellites from Jason-1, Jason-2, and Jason-3.**

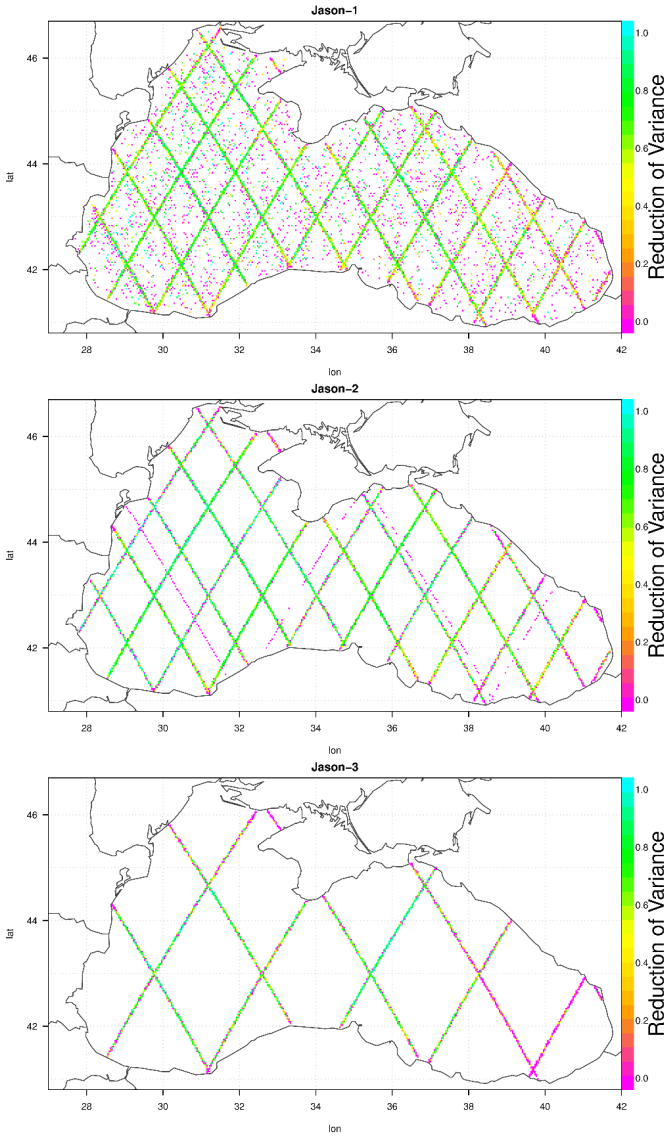


**Figure 17: Reduction of Variance RV derived from significant wave heights simulated in WAM and from individual satellite measurements.**

## V EXAMPLES

The following figures present results demonstrating the capabilities of the long-term reanalysis. Note that the empirical orthogonal functions in figures 26-29 have been computed on a slightly coarser grid due to computational demand.

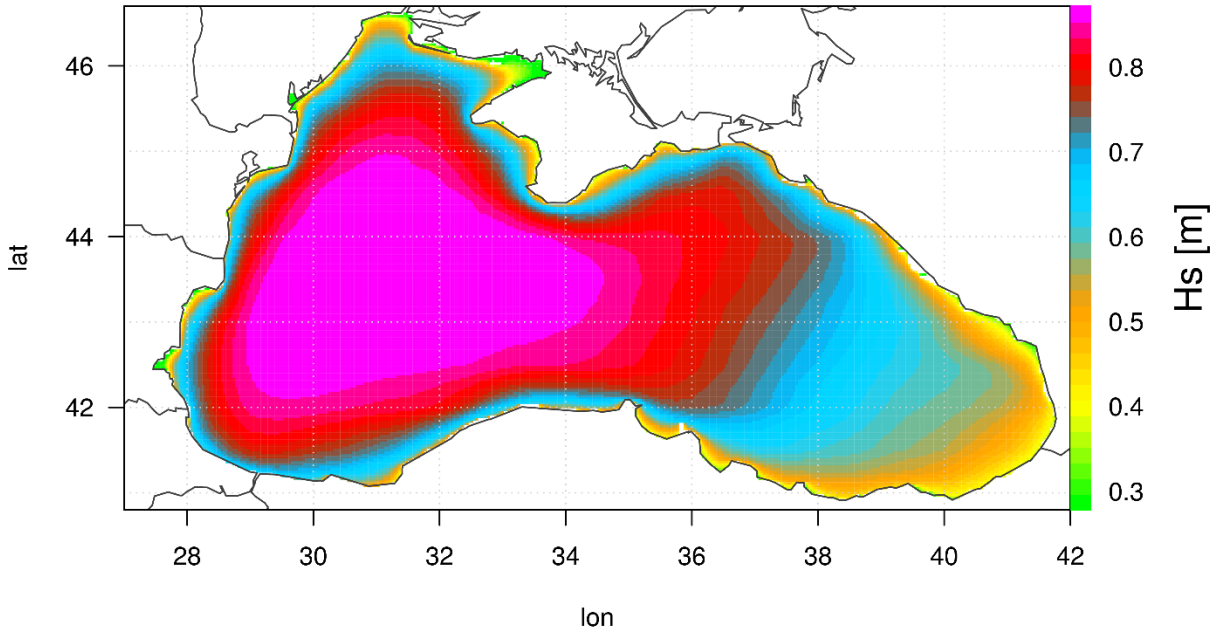


**Figure 18: Average significant wave height in WAM calculated over the period 2002-2017.**

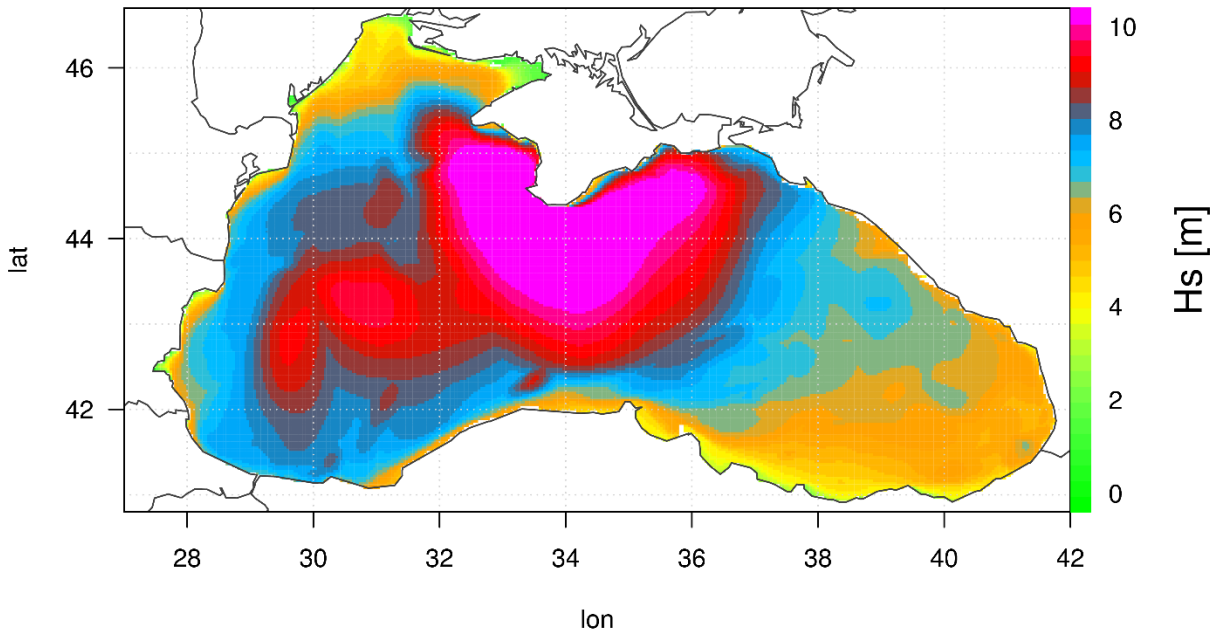


**Figure 19: Maximum significant wave height in WAM calculated over the period 2002-2017.**

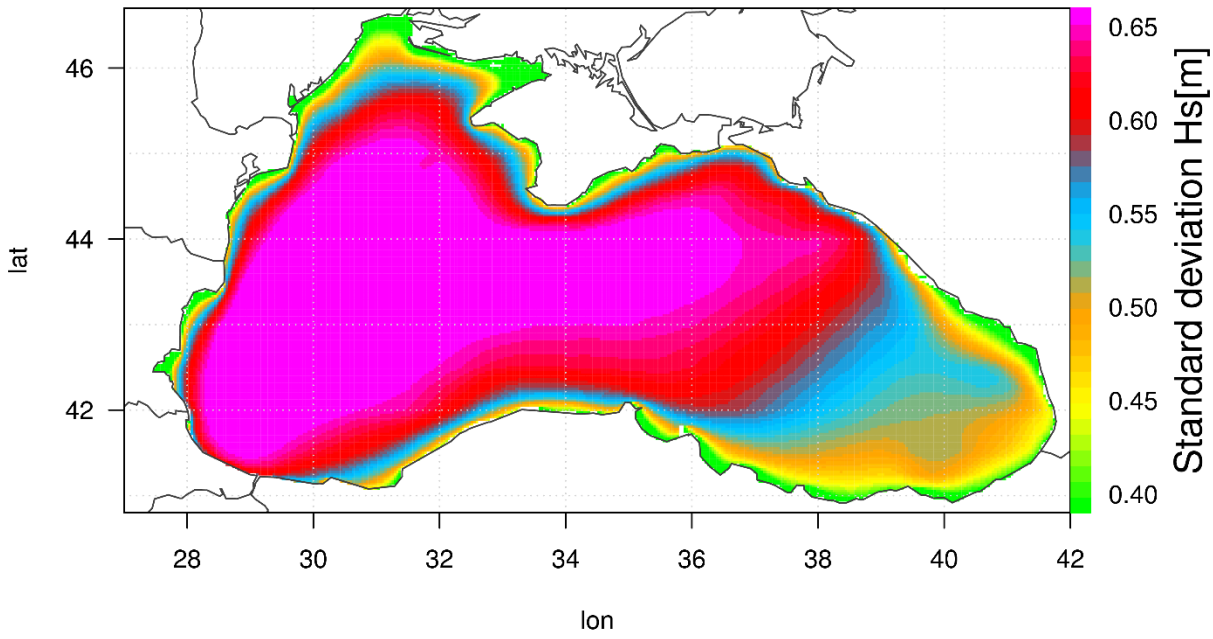


**Figure 20: Standard deviation of the significant wave height in WAM calculated over the period 2002-2017.**

.

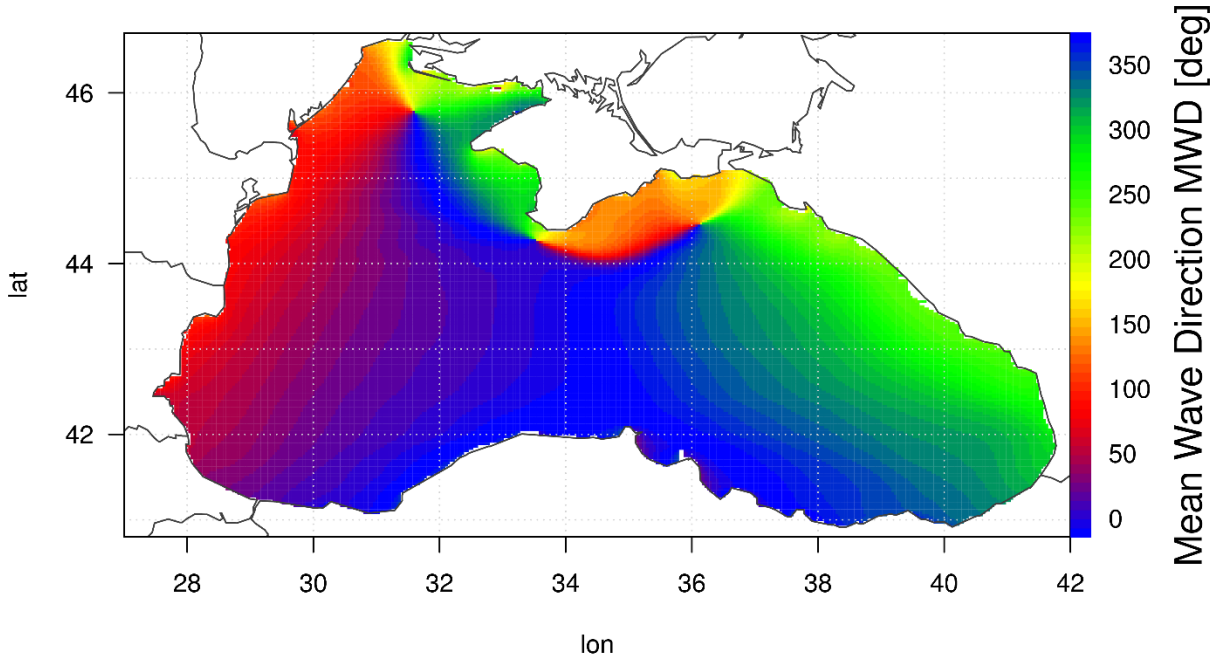


**Figure 21: Average mean wave direction in WAM calculated over the period 2002-2017.**

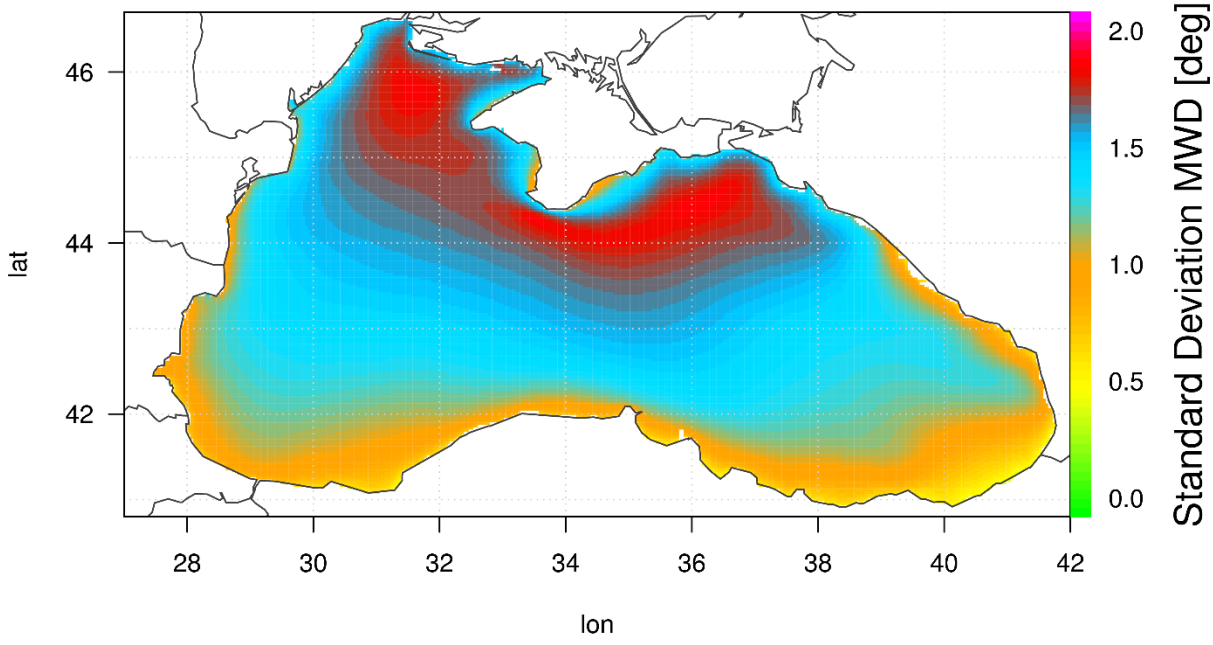


**Figure 22: Standard deviation of the mean wave direction in WAM calculated over the period 2002-2017.**

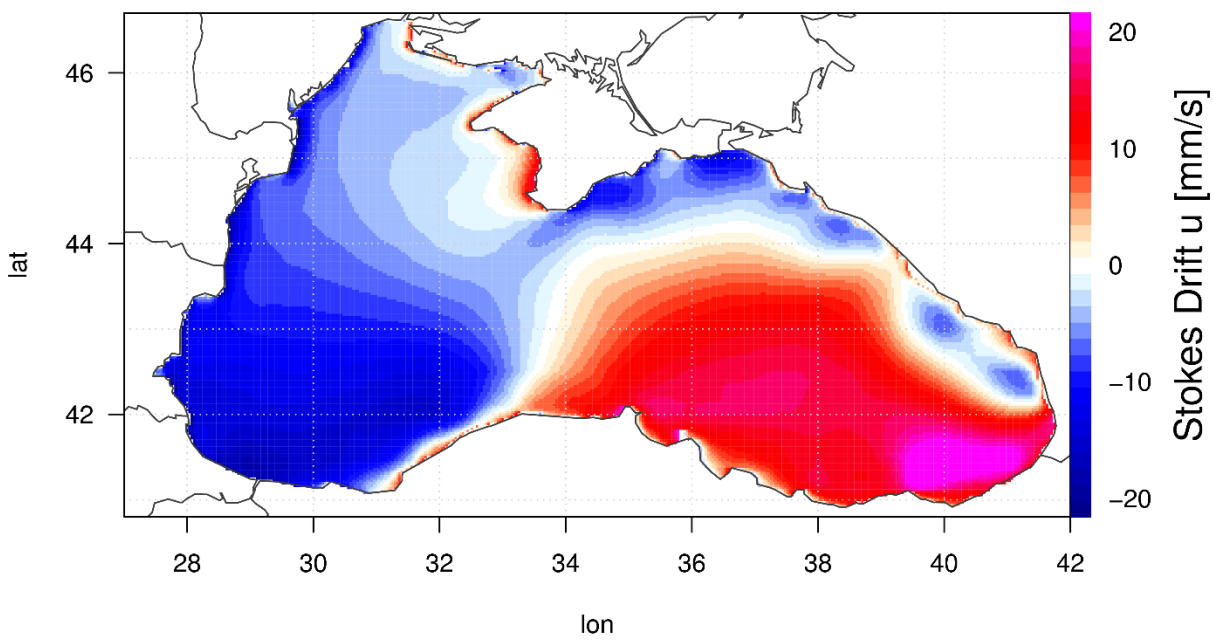


**Figure 23: Average u-component of the Stokes drift in WAM calculated over the period 2002-2017.**

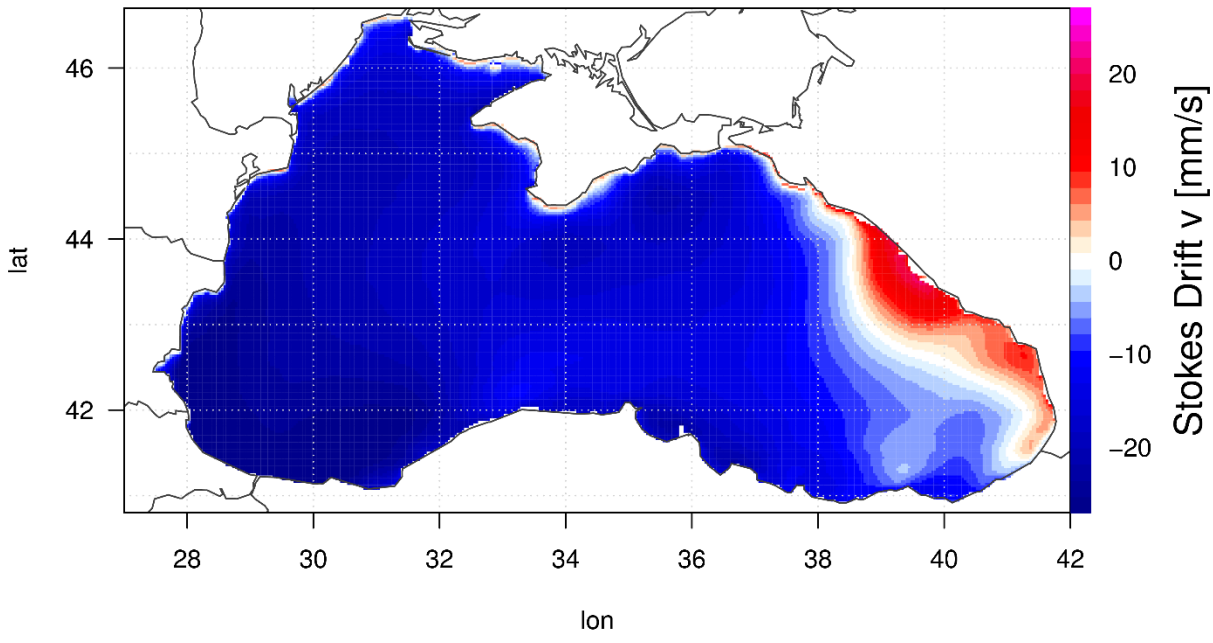


**Figure 24: Average u-component of the Stokes drift in WAM calculated over the period 2002-2017.**

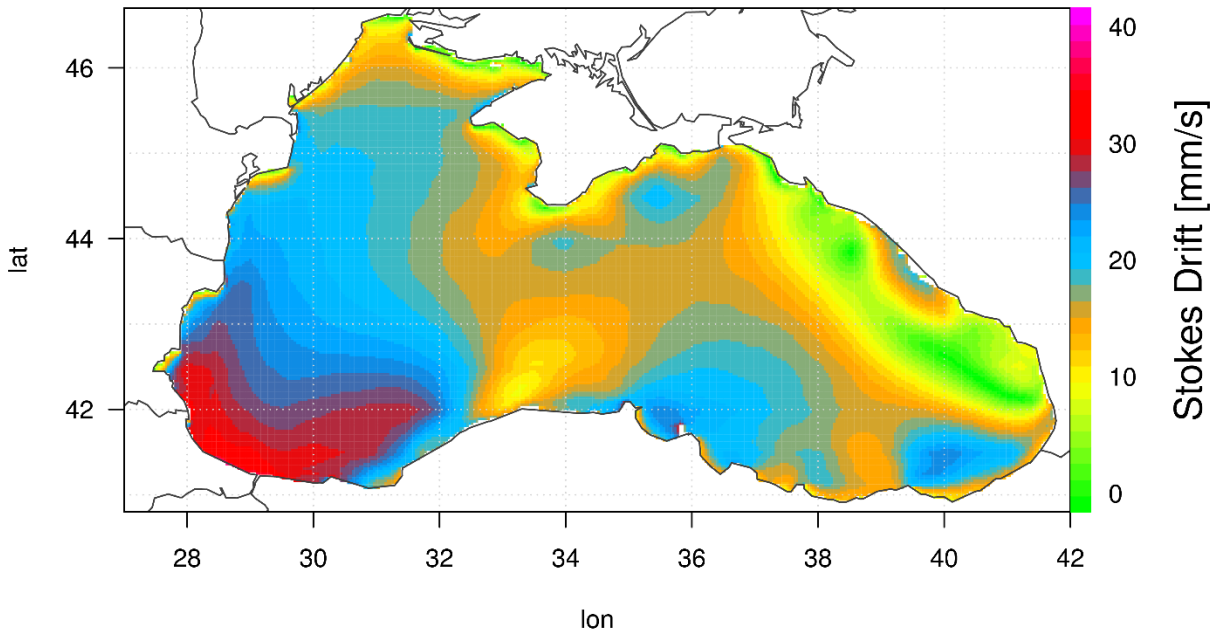


**Figure 25: Average Stokes drift in WAM derived from the average of u- and v-components (shown in figure 21 and 22) calculated over the period 2002-2017.**

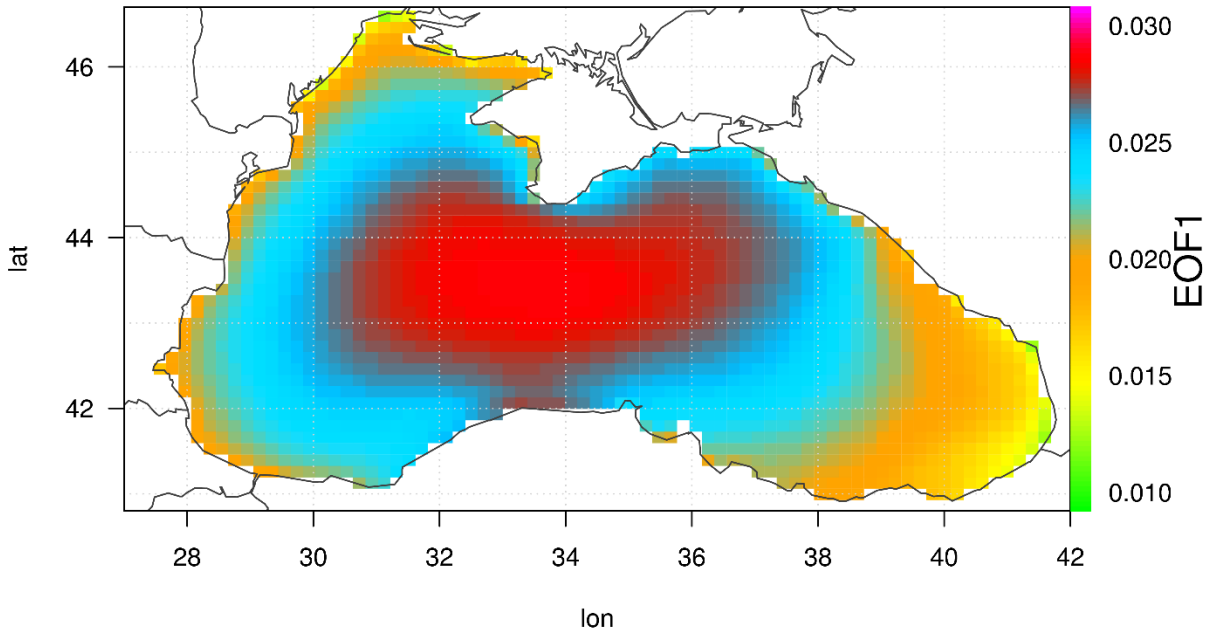


**Figure 26: Eigenvector of the first empirical orthogonal function (EOF1). The EOF1 is representative for 61.2 % of the variance.**

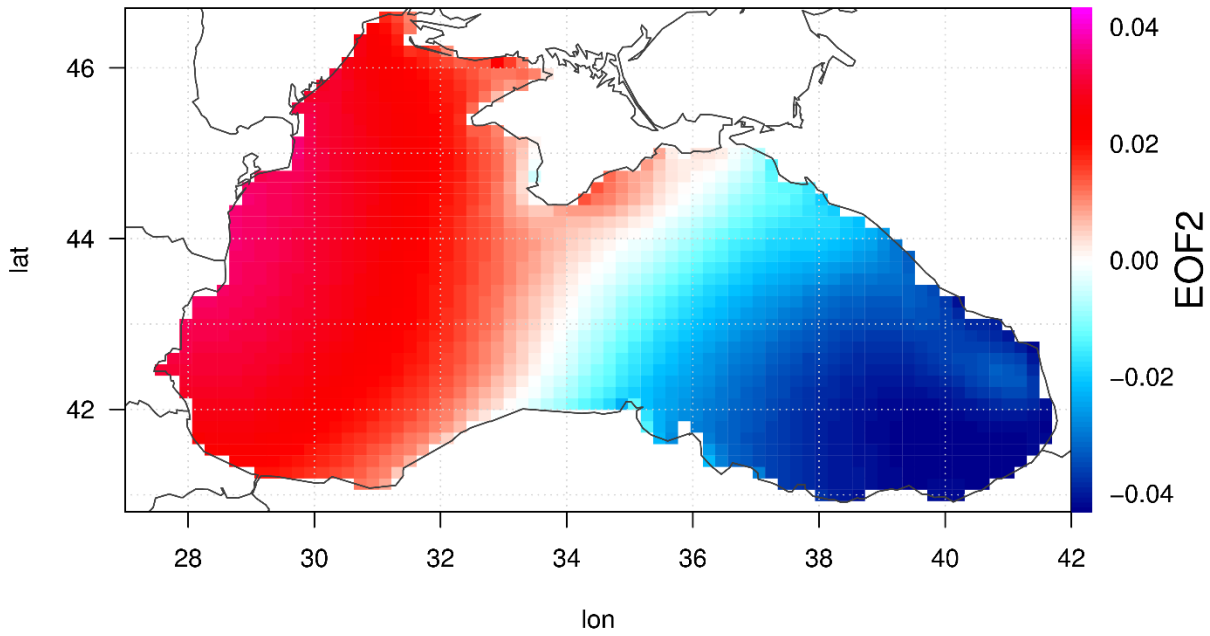


**Figure 27: Eigenvector of the second empirical orthogonal function (EOF2). The EOF2 is representative for 16.3 % of the variance**

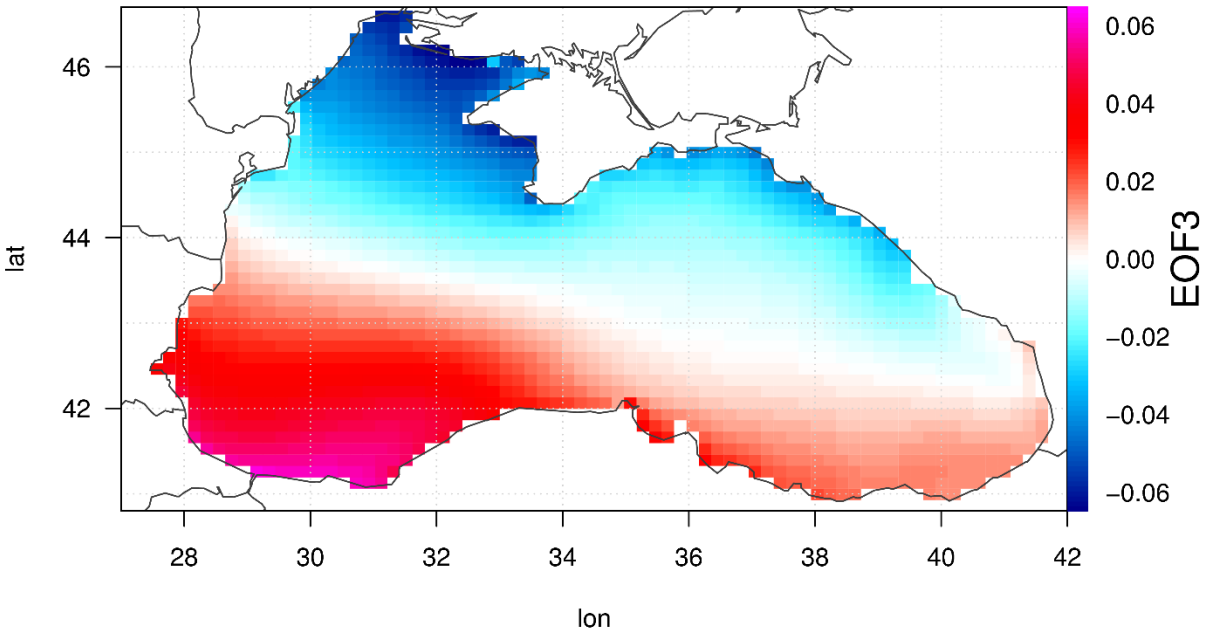


**Figure 28: Eigenvector of the third empirical orthogonal function (EOF3). The EOF3 is representative for 6.2 % of the variance.**

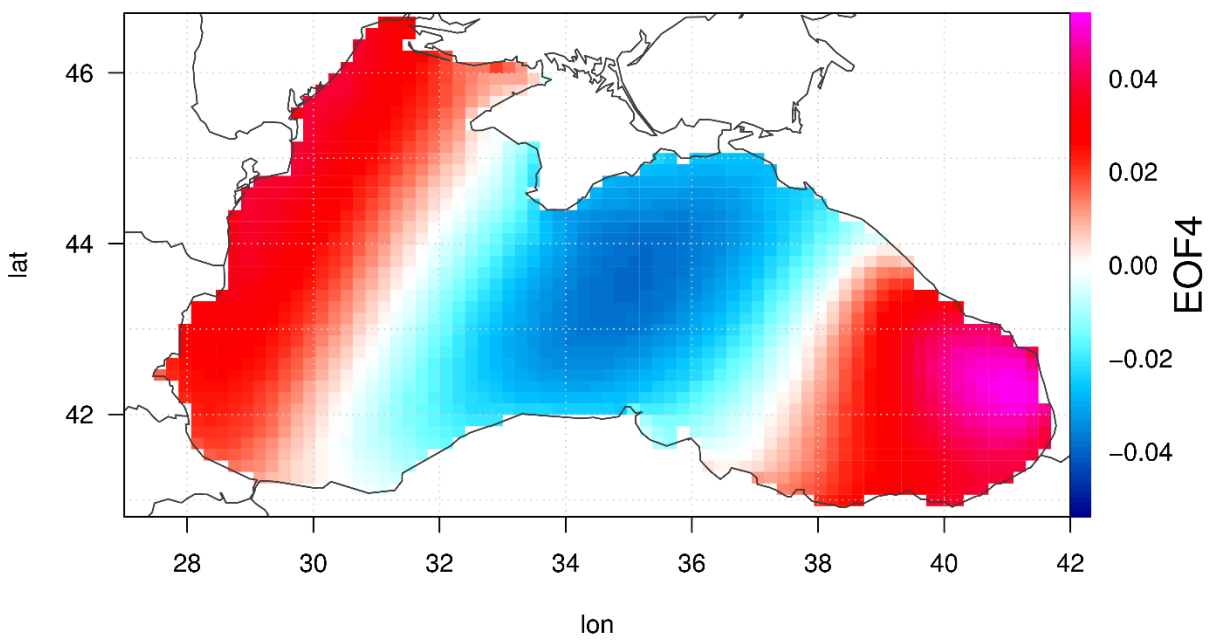


**Figure 29: Eigenvector of the fourth empirical orthogonal function (EOF4). The EOF4 is representative for 4.6 % of the variance.**

## VI SYSTEM'S NOTICEABLE EVENTS, OUTAGES OR CHANGES

The BLKSEA_REANALYSIS _WAV_007_006 reanalysis a new product. There is no previous version available.

## VII QUALITY CHANGES SINCE PREVIOUS VERSION

The BLKSEA_REANALYSIS _WAV_007_006 reanalysis a new product. There is no previous version available.

## VIII REFERENCES

Arkhipkin VS, FN Gippius, KP Koltermann, GV Surkova (2014) Wind waves in the Black Sea: results of a hindcast study, Nat. Hazards Earth Syst. Sci., 14, 2883-2897, doi:10.5194/nhess-14-2883-2014

Breivik, Ø, J-R Bidlot, P A Janssen (2016) A Stokes drift approximation based on the Phillips spectrum, Ocean Model, 100, 49-56, doi:10.1016/j.ocemod.2016.01.005

Breivik, Ø, P Janssen, and JR Bidlot (2014) Approximate Stokes Drift Profiles in Deep Water, J Phys Oceanogr, 44(9), 2433–2445, arXiv:1406.5039, doi:10.1175/JPO-D-14-0020.1

Behrens, A. (2015) Development of an ensemble prediction system for ocean surface waves in a coastal area. Ocean Dynamics, Volume 63, Issue 4 (2015), pp 469-486 DOI10.1007/s10236-015-0825-y

Chawla A, Spindler DM, Tolman HL (2013) Validation of a thirty year wave hindcast using the Climate Forecast System Reanalysis winds, Ocean Modelling, 70, pp 189-206, doi: 10.1016/j.ocemod.2012.07.005.

Dimitrova M, Kortcheva A, Galabov V (2013) Validation of the operational wave model WAVEWATCH III against altimity data from Jason-2 satellite, Bul. J. of Meteo & Hydro 18/1-2 : 4-17.

ECMWF (2015) IFS Documentation CY41R1, Book Chapter, ECMWF.

Günther H, Hasselmann S, Janssen PAEM (1992) The WAM Model Cycle 4.0. User Manual. Technical Report No. 4, Deutsches Klimarechenzentrum, Hamburg, Germany. 102 pages.

Hersbach H, Janssen PAEM (1999) Improvements of the short fetch behaviour in the WAM model. J Atmos Oceanic Tech 16: 884-892.

Janssen PAEM (2008) Progress in ocean wave forecasting. J Comput Phys 227:3572-3594.

Kenyon KE (1969) Stokes Drift for Random Gravity Waves. JGR, Vol 74, No 28 : 6991-6994

Komen GJ, Cavaleri L, Donelan M, Hasselmann K, Hasselmann S, Janssen PAEM (1994) Dynamics and Modelling of Ocean Waves, Cambridge University Press.

Kortcheva A, Dimitrova M, Galabov V (2009) A wave prediction system for real sea state forecasting in Black Sea, Bul. J. of Meteo & Hydro Vol. 1 : 1-16.

Kourafalou V., De Mey P., Staneva J., Ayoub N., Barth A., Chao Y., M Cirano M, et al., 2015. Coastal Ocean Forecasting: science foundation and user benefits, Journal of Operational Oceanography8, 147.,

WAMDI group: Hasselmann S, Hasselmann K, Bauer E, Janssen PAEM, Komen GJ, Bertotti L, Guillaume A, Cardone VC, Greenwood JA, Reistad M, Zambreski L, Ewing J (1988) The WAM model – a third generation ocean wave prediction model, J Phys Oceanogr 18: 1775-1810.

Samedo, A., Weisse, R., Behrens, A., Sterl, A., Bengtsson, L. and Günther, H. (2013): Projection of global wave climate change towards the end of the 21st century, Journal of Climate (AMS – American Meterological Society), Vol 26, pp 8269-8288

Staneva J, Alari V, Breivik O, Bidlot J-R, Mogensen K (2016) Effects of wave-induced forcing on a circulation model of the North Sea. Ocean Dynamics, DOI 10.1007/s10236-016-1009-0

Staneva J, Wahle K, Koch W, Behrens A, Fenoglio-Marc L, Stanev E (2016) Coastal flooding: impact of waves on storm surge during extremes – a case study for the German Bight, Nat. Hazards Earth Syst. Sci., 16, 2373-2389, doi:10.5194/nhess-16-2373-2016Staneva,

Staneva J., Wahle K. Günther H. and Stanev E., (2016) Coupling of wave and circulation models in coastal-ocean predicting systems: OS-2015-86, Special Issue: Operational oceanography in Europe 2014 in support of blue and green growth, 12, 3169–3197.

Staneva, J, Wahle K, Koch W, Stanev E., Fenoglio-Marc, (2016) Surge and wave predictions: Wave-current interaction during extremes in the German Bight, Ocean Science.

Staneva, J., A. Behrens and Wahle K., (2015) Wave modelling for the German Bight coastal-ocean predicting system, Journal of Physics: Conference Series, 633, pp 233-254, doi:1211, 0.1088/1742-6596/633/1/012117, ISBN: 978-3-939230-28-1

Stanev, E.V., Y. He, J. Staneva and E. Yakushev (2014) Mixing in the Black Sea detected from the temporal and spatial variability of oxygen and sulfide – Argo float observations and numerical modelling. Biogeosciences, 11, 5707–5732

Staneva, J., Behrens, A. and Groll, N. (2014) Recent Advances in Wave Modelling, Die Küste 81/2014, 233 – 254

Venables, W. N. and Ripley, B. D. (2002) Modern Applied Statistics with S, Fourth edition, Springer

Wahle K., Staneva J., Guenther H., (2015) Data assimilation of ocean wind waves using Neural Networks. A case study for the German Bight, Ocean Modelling, pp. 117-125

WAMDIG (1988) The WAM model - A third generation ocean wave prediction model. Journal of Physical Oceanography, 18, 1775-1810.